

Pediatric Malignancies

12

Helen Nadel, Barry Shulkin, Zvi Bar-Sever,
and Francesco Giammarile

12.1 General Tracer-Related Parameters

Radiopharmaceutical and Administered Activity

The EANM pediatric dosage card and to the North American consensus guidelines on radiopharmaceutical administration in children in the respective EANM and SNMMI and image gently web sites should be followed [1, 2].

Reference to national regulation guidelines, if available, should be considered.

H. Nadel (✉)
Lucile Packard Children's Hospital Stanford
University, Palo Alto, CA, USA

B. Shulkin
Department of Diagnostic Imaging, St. Jude
Children's Research Hospital, Memphis, TN, USA

Z. Bar-Sever
Schneider Children's Medical Center of Israel, Tel
Aviv University, Petah Tiqva, Israel

F. Giammarile
Nuclear Medicine and Diagnostic Imaging Section,
Division of Human Health, Department of Nuclear
Sciences and Applications, International Atomic
Energy Agency, Vienna, Austria

Box 12.1 FDG Imaging Protocol [3–6]

Patient Preparation

- Fast: 4 h before tracer injection and during the uptake.
- Good hydration with plain, unflavored water is allowed and encouraged.
- Measure and record patient's height and weight on the day of the exam.
- Avoid strenuous exercise 24 h prior to scan.
- Discontinue glucose-containing IV fluids and parenteral nutrition from midnight before test or minimum of 6 h.
- Blood glucose level must be measured before radiotracer administration and should be below 200 mg/dL (11.1 mmol/L), preferably below 120 mg/dL (6.66 mmol/L).
- Date of last dose of potentially interfering medications that may cause false positive and false negative altered bio-distribution should be recorded in technologist/ study notes (see below in study interpretation).
- Brown fat reduction techniques include:
 - Early arrival (30–45 min prior to planned radiotracer injection time) to settle patient, establish IV line, and warm the patient in a temperature-controlled room with the addition of warm regular or electric blankets.

- Avoid cold and air-conditioned spaces in transportation prior to study.
- Premedication such as benzodiazepines and beta-adrenergic blockers (oral propranolol, IV fentanyl, oral diazepam in moderate dose) may be carefully used as a second option in consultation with referring physicians and pediatric anesthetists.

Radioisotope:

- [¹⁸F]-Fluorodeoxyglucose (FDG)

Activity:

- 3.7–5.2 MBq/kg (0.10–0.14 mCi/kg), minimum dose 26 MBq (0.7 mCi).

Refer to the EANM pediatric dosage card and to the North American consensus guidelines on radiopharmaceutical administration in children in the respective EANM and SNMMI and image gently web sites.

Reference to national regulation guidelines, if available, should be considered.

- FDG activity can be reduced when using modern PET technology, to 0.06–0.08 mCi/kg 2.46–2.96 MBq/kg [7].

Acquisition Protocol

- Uptake time: 60 min ($\pm 10\%$) between injection and scanning.
- Patients should not talk, text, play video games, chew gum, or suck candies during the uptake phase.
- Diapers should be changed in infants before the scan.
- Acquisition parameters: 2–4 min/bed position (depending on equipment).

Study Interpretation for FDG Imaging [8–10]

- Standardized elements to include in the PET/CT report can be found at the SNMMI website

http://interactive.snm.org/docs/PET_PROS/ElementsofPETCTReporting.pdf

- Abnormally increased FDG uptake should be described with respect to:
 - Intensity: mild, moderate, or severe, or compared to the blood pool and liver activity.
 - Pattern: focal, diffuse, linear.
 - Localization: based on CT or MRI.
- Physiological tracer distribution, including specific patterns in children: brain, salivary glands, lymphatic tissue of the Waldeyer's ring, muscles, brown fat, myocardium, mediastinum, thymus, liver, kidneys and bladder, gastrointestinal tract, testis, uterus, and ovaries.
- False positives, including specific patterns in children:
 - Infant mouth with feeding or sucking during the uptake phase.
 - Thymus: uptake decreases with age but may increase after chemotherapy, thymic rebound.
 - Brown fat: usually bilateral in the neck, supraclavicular regions, axillae, mediastinum, paravertebral regions, and perinephric areas. Infradiaphragmatic activity considered to be brown fat is seen, as a rule, in conjunction with supradiaphragmatic brown fat.
 - Diffuse uptake in bone marrow following hematopoietic stimulating drugs such as G-CSF.
 - Increased uptake in infectious and inflammatory processes, and in other benign entities.
 - Uptake in post-surgical scars.
 - Uptake in growth plate.
- False negatives:
 - Hyperinsulinemia and hyperglycemia.
 - Small lesions, with limited tracer avidity.
 - Low metabolic tumors are rare in children but may occur with differentiated thyroid cancer and well-differentiated NETs.
 - Tumor necrosis.
 - Recent radiation or chemotherapy.
 - Recent treatments such as high-dose corticosteroid therapy and anti-retroviral medication.

Box 12.2 Radioiodinated Meta-iodobenzylguanidine (MIBG) Imaging Protocol [11, 12]

Patient Preparation

- Administer thyroid-blocking medication.
- LUGOL solution:
 - Starting 2 days prior to and continued for 3 days after injection.
 - Dose: 0.6 mL of 5 % solution/day, single dose or split into 2 × 0.3 mL doses.
 - Delivery: diluted in any drink such as milk or juice as may cause a burn in the throat if undiluted.
- Supersaturated potassium iodide (SSKI):
 - Starting 30–60 min prior to tracer administration, on day 0 and continued for a week.
 - Dose: <1 month—one drop orally/day; 1 month—3 years: 2 drops orally/twice a day; 3–18 years of age: 3 drops orally/three times a day; ≥70 kg—adult: 6 drops orally (2 drops/3 times a day).
- Potassium iodate (in individuals sensitive to iodine and if no other thyroid blockade is available).
 - Starting 1 h prior to tracer injection, up to 5 times within the next 36 h.
 - Dose: 10 mg/kg, maximum 500 mg, minimum 50 mg.
 - Delivery: 200 mg tablet can be crushed, dissolved in 2 mL of sterile water, and administered by syringe or placed on a sugar lump.

Radiopharmaceuticals

- [¹²³I]-MIBG—the current standard SPECT tracer.
- [¹³¹I]-MIBG—should only be used if ¹²³I-MIBG or an alternative PET tracer is not available.

Activity

- ¹²³I-MIBG: North American consensus guidelines recommend a dose of 5.2 MBq/kg (0.14 mCi/kg), minimum dose of 37 MBq (1 mCi), and maximum dose of 370 MBq (10 mCi). The EANM pediatric dosage card recommends a slightly higher activity, minimum dose of 37 MBq (1 mCi), and maximum dose of 400 MBq (10.8 mCi).
- ¹³¹I-MIBG: minimum injected dose of 35 MBq (0.95 mCi) and maximum dose of 78 MBq (2.11 mCi).

Acquisition Protocols

¹²³I-MIBG:

- Time of scan: 24 h post-injection. Rare images at 48 h are added to clarify sites with low-grade uptake.
- Collimator: medium energy is preferred, reduces scatter and septal penetration of high-energy photons; low energy can be also used.
- Planar scans:
 - In older children: whole-body anterior and posterior projections, 5 cm/min, minimum 30 min, matrix 1024 × 512 or 1024 × 256.
 - In young children: multiple spot views of the entire body are preferred, matrix 256 × 256, trunk: 10 min/500 Kcounts. Limbs and skull 100 Kcounts, skull (anterior, posterior, left and right lateral views).
 - SPECT: 120 projections, 25–35 s/step, matrix 128 × 128, iterative reconstruction.
- SPECT/CT, when available, is recommended.

¹³¹I-MIBG:

- Time of scan: 48 h post-injection, possible supplements at 72 h.

- Collimator: high energy or medium energy.
- Planar scans: whole body, anterior and posterior images, scan speed 4 cm/min, or multiple spot views of the entire body (150 Kcounts/view).
- SPECT and SPECT/CT as indicated.

Study Interpretation for MIBG Imaging [11, 13, 14]

- Physiological biodistribution: myocardium, salivary and lacrimal glands, liver, lungs (blood pool on early images), bowel, renal collecting system, uterus (during menstrual period).
 - Adrenal glands: symmetric, mild (\leq to the liver), normal size on CT.
 - Brown fat.
 - Thyroid (uptake of free iodine in case of poor blockade).
- False positives:
 - Lung atelectasis, pneumonia.
 - Heterogeneous liver uptake (including focal uptake in the left lobe).
 - Kidneys and/or dilated ureters.
 - Rare-vascular malformations, accessory spleen, ectopic kidneys, foregut duplication, hemorrhagic cysts, ovarian torsion, and hernia.
- False negatives:
 - MIBG-negative neuroblastoma (10% of cases)
 - MIBG-negative metastases
 - Small lesions, below the camera resolution

Box 12.3 [¹⁸F] Fluoro-Dihydroxyphenylalanine (FDOPA) Imaging Protocol [11, 15]

Patient Preparation

- Fast: 4 h
- Adequate hydration

- Drug withdrawal (48 h prior to tracer administration): aromatic L-amino acid decarboxylase (AADC), catechol-o-methyl transferase (COMT), and monoamine oxidase (MAO) inhibitors.
- Premedication with carbidopa: if used in children a dose of 2 mg/Kg is administered 1 h before FDOPA injection.

Activity

- 3 MBq/Kg (0.08 mCi/Kg), minimum dose is 26 MBq (0.7 mCi).

Acquisition Protocol

- Uptake time: 60–90 min.
- Acquisition parameters: 3 min/bed position.

Study Interpretation for FDOPA Imaging [16, 17]

- Physiologic biodistribution:
 - High: basal ganglia, liver, adrenals, pancreas (variable).
 - Moderate: myocardium, skeletal muscles, growth plate.
 - Faint: breasts, oral cavity, esophagus, bowel.
 - Excretion: biliary (gallbladder and biliary tract) and urinary (kidneys, ureters, urinary bladder).
- False positives:
 - Physiologically intense, variable uptake in uncinate process of pancreas.
 - Stasis in small intrahepatic bile ducts and/or in the urinary system.
 - Growth plate fractures.
- False negative:
 - Lesions adjacent to sites with high physiologic uptake.
 - Small lesions.
 - Lesions with low tracer avidity.

Box 12.4 [⁶⁸Ga]-Peptides Imaging Protocol [15]

Patient Preparation

- No fasting requiring.
- Drug withdrawal: therapy with short-/long-acting somatostatin analogues (rare in children)—to avoid possible somatostatin receptor (SSTR) blockade.
- Short-acting: 1–2 days discontinuation.
- Long-acting: 4–6 weeks discontinuation.

Radiopharmaceuticals

- ⁶⁸Ga-DOTA-TATE, -TOC, -NOC.

Activity

- 2 MBq/kg (0.054 mCi/kg), minimum dose is 14 MBq (0.3 mCi).

Acquisition Protocol

- Uptake time: 60 min (range 45–90 min)
- Field-of-view (FOV): true vertex-to-toe
- Acquisition parameters: 2–4 min/bed position

Study Interpretation for ⁶⁸Ga-Peptide Imaging [18, 19]

- Physiologic biodistribution:
 - High uptake: pancreas (uncinate process), spleen, kidneys, pituitary gland.
 - Moderate uptake: liver, salivary glands, thyroid, bowel.
 - Faint uptake: adrenals, prostate, breast.
- False positives:
 - Physiologic uptake in uncinate process, accessory spleens, splenosis, epiphyseal growth plates.
 - Meningiomas.
 - Skeletal lesions such as fractures, vertebral hemangioma, fibrous dysplasia.
 - Inflammatory processes such as reactive

lymph nodes, post-radiation therapy changes.

- Urine contamination.
- False negatives:
 - Small lesions.
 - Lesions adjacent to sites with high physiologic uptake.
 - Tumors with low or variable SSTR expression.
 - Lesion dedifferentiation.

Box 12.5 Bone Imaging Protocols [20–24]

Patient Preparation

- No need to fast.
- No need for medication withdrawal.
- Good hydration.
- Frequent bladder emptying between injection and delayed imaging, and immediately before scanning.
- Change diapers immediately before scanning.

Radiopharmaceuticals

- [^{99m}Tc]Tc-methylene diphosphonate (MDP) or similar diphosphates.
- [¹⁸F]sodium fluoride (NaF)

Activity

- MDP: 9.3 MBq/kg (0.25 mCi/Kg), minimum dose 37 MBq (1.0 mCi).
- NaF 2.22 MBq/kg (0.06 mCi/kg), minimum dose 14 MBq (0.4 mCi).

Refer to the EANM pediatric dosage card and to the North American consensus guidelines on radiopharmaceutical administration in children in the respective EANM and SNMMI and image gently web sites.

Reference to national regulation guidelines, if available, should be considered.

Acquisition Protocols

Bone scintigraphy

- Position: supine, comfortably secured to the bed.
- Collimators: high- or ultrahigh low energy, parallel hole collimator.
- Time of scanning: at 2–4 h post-injection.
- Acquisition parameters:
- Whole body sweeps with bed speed adjusted to the child's age.
 - 8 cm/min for ages 4–8 years.
 - 10 cm/min for ages 8–12 years.
 - 12 cm/min for ages 12–16 years.
 - 15 cm/min over 16 years of age.
- Alternative: multiple spot views over entire skeleton, anterior and posterior projections, matrix 256 × 256, counts: torso 500 Kcounts, skull 300 Kcounts, knees 100–200 Kcounts, hands and feet 50–100 Kcounts.
- SPECT 120 projections, 15–30 s/view, matrix 128 × 128 should be included:
 - To areas of localized symptoms.
 - If an abnormality is detected on planar imaging.
- SPECT/CT, if available should replace SPECT [25].
 - For the CT component of SPECT/CT—tube setting will depend on whether the CT is intended to be low dose or fully diagnostic.
- Delayed 24-h scan can be performed:
 - In cases of uncertain findings on routine 3-h scintigraphy.
 - When residual bladder activity overlies the pelvis and the child refuses to urinate or when bladder emptying is incomplete.

Bone NaF PET/CT:

- Time of imaging: at 30–45 min after tracer injection.
- Position: supine; arms by the sides for whole-body imaging, elevated when only the axial skeleton is scanned.
- Acquisition parameters: 2–5 min /bed position, varies depending on injected amount, BMI, and camera.

Study Interpretation for Bone Imaging

- Physiologic tracer biodistribution:
 - Homogeneous throughout the entire skeleton.
 - Visualization of kidneys, ureters, bladder.
 - Increased uptake in metaphyses of children and adolescents.
- Abnormally increased skeletal uptake should be described with respect to:
 - Intensity higher or lower than in adjacent or in corresponding contralateral bone.
 - Pattern: focal or diffuse.
 - Location and number of foci.
 - Patterns of ST uptake:
 - Diffuse decreased: due to increased heterogeneous uptake in bone.
 - Diffuse increased: renal failure, short uptake time, of significant tracer extravasation at the injection site.
 - Focal increased: infection/inflammation, trauma, (calcified) ST metastasis.
- Pitfalls
 - Urinary contamination or diversion reservoirs
 - Injection artifacts
 - Patient motion
 - Faulty energy window for image acquisition

12.2 Lymphoma and Sarcoma

Clinical Indications—Imaging with FDG (see also Box 12.1) [22, 26–29]

- Staging/restaging
- Metastatic workup in sarcoma
- Response assessment
- End of therapy baseline
- Biopsy site planning
- Confirmation of equivocal or discrepant findings on other imaging studies

Specific Study Interpretation Criteria

Lymphoma [30]

- The (Deauville) five-point scale can be used in the assessment of treatment response in HL and NHL.
 - Score 1: No uptake above the background.
 - Score 2: Uptake \leq mediastinum.
 - Score 3: Uptake $>$ mediastinum but \leq liver.
 - Score 4: Uptake moderately increased compared to the liver at any site.
 - Score 5: Uptake markedly increased compared to the liver at any site.
 - Score X: New areas of uptake unlikely to be related to lymphoma.

Sarcoma [31–33]

- Reduction in standard uptake values (SUV) max from baseline of greater than 50% has been associated with overall improved progression-free survival.

Correlative Imaging [34]

- Chest radiograph may be the first examination in a child presenting with chest/ mediastinal symptoms and can identify mediastinal mass and possible tracheal compression.
- US of the abdomen and pelvis may identify lymphadenopathy but is not adequate for staging purposes. Cross-sectional imaging with contrast-enhanced CT and or MRI will be the next cross-sectional imaging study.
- PET/CT and/or PET/MRI may be performed as next cross-sectional imaging in some institutions without intermediate stand-alone CT or MRI study.
- In suspected sarcoma radiographs will be the first study in a child presenting with focal pain. Cross-sectional imaging with contrast-enhanced CT and dedicated high-resolution MRI will follow.

Red Flags

- Good hydration prior to tracer administration will accelerate and increase excretion of the excess radiotracer.
- If blood glucose levels are above 200 mg/dL (11.1 mmol/L), the study should be rescheduled, if possible. In diabetic patients, consultation with treating endocrinologist can be helpful in case of complex diabetic or insulin requirements.
- Check the quality of images and of factors that may influence the SUV before reporting.
- Study scheduling: in patients after treatment the study should be ideally scheduled at least 14 days after the last course of chemotherapy, and 2 months after surgery and 3 months after radiotherapy.
- Semiquantitative analysis, in particular, SUV measurements, should be used with caution.
- PERCIST criteria have not been validated in children.
- FDG-PET is recommended in surveillance of lymphoma only in selected cases, determined by clinical situation [30].
- Base of the skull to mid-thigh examination has been found sufficient in patients with lymphoma [35].
- Staging scans performed after the initiation of treatment may result in false-negative studies [36].

Take Home Messages

- FDG is taken up by malignant cells via glucose membrane transporters and phosphorylated by hexokinase into FDG-6-Phosphate, which does not follow further enzymatic pathways and accumulates proportionally to the glycolytic cellular rate.
- Fasting decreases serum glucose levels and maintains a low insulin level.
- The 60 min uptake time is needed for absorption and clearance of the radiotracer.

- Patients should not talk, text, play video games, chew gum, or suck candies during the uptake phase to avoid FDG uptake in tense muscles.
- PET imaging for staging in pediatric lymphoma should be given high priority for scheduling pre-therapy, especially in patients with critical condition.
- Whole-body PET studies, from vertex to toes, should be performed in sarcoma and most of the pediatric solid cancers since the

diseases can often occur distal to elbows and knees.

Representative Case Examples

Case 12.1 Diffuse Large B-cell Non-Hodgkin's Lymphoma (NHL), Staging (Fig. 12.1)

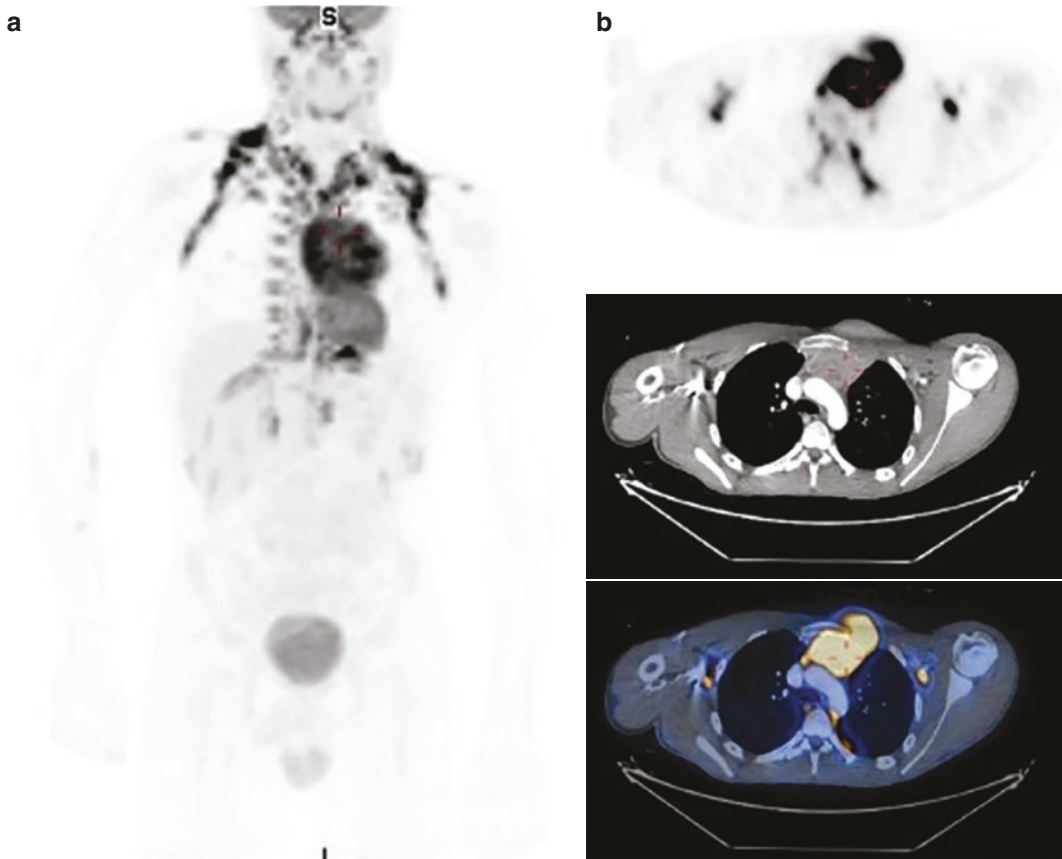


Fig. 12.1 History: An 18-year-old boy with diffuse large B-cell NHL was referred for staging. Study report: FDG-PET MIP (a) and selected PET, CT, and PET/CT transaxial slices at the level of the upper chest (b) show an area of intense, inhomogeneous, abnormal tracer uptake in a 9 × 9 cm mass in the anterior mediastinum, involving the ST and bone, specifically the left 1–4 ribs and sternum, with suspected involvement of the left lung. Note physiological cervical and axillary uptake in brown fat. There are no other sites of nodal hypermetabolism in the neck and chest, and no pulmonary nodules. There is no nodal

hypermetabolism in the retroperitoneal or pelvic lymphatic chains. The spleen is normal in size and tracer avidity. There is focal increased physiological tracer uptake in paraspinial and right suprarenal brown fat. There are no areas of abnormal uptake in the appendicular and axial skeleton. Impression: The findings are consistent with lymphoma of the mediastinum involving bony structures and possibly the left lung. The patient received four courses of chemotherapy and a repeat FDG-PET/CT study (not shown) demonstrated a complete metabolic response

Case 12.2 Burkitt's Non-Hodgkin's Lymphoma (NHL)—Staging (Fig. 12.2)

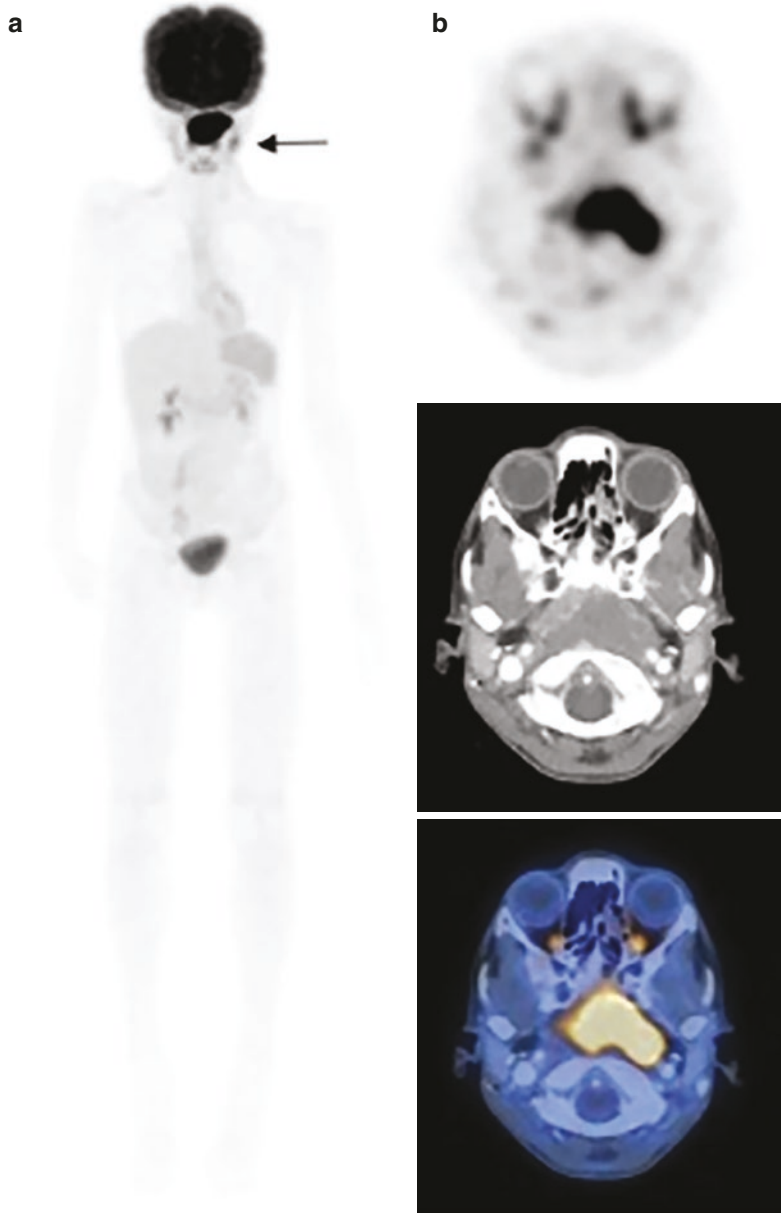


Fig. 12.2 History: A 9-year-old boy with newly diagnosed Burkitt's NHL following biopsy of the nasopharynx was referred for staging. Study report: FDG-PET MIP (a) and selected transaxial slices PET, CT, and PET/CT of the head (b) show intense pathological tracer uptake in a mass involving the nasopharynx, the oropharynx, and the base of the skull. Low-to-medium intensity uptake (SUVmax 2.24–5.51) is noted in 8 mm cervical lymph nodes, more prominent on the left. There is no nodal hypermetabolism in the chest and no pulmonary nodules. There is no nodal hypermetabolism in abdominal, retroperitoneal, or pelvic

lymphatic chains. The spleen is normal in size, with homogenous, mildly increased tracer avidity. There are no areas of abnormal uptake in the appendicular and axial skeleton. Impression: The findings are consistent with lymphoma involving the nasopharynx and possibly cervical nodes, mainly on the left side of the neck. Low-intensity activity in additional cervical lymph nodes can be related to an inflammatory reaction. Diffuse, homogenous tracer activity in the spleen, most probably due to increased hematopoiesis or an inflammatory reaction

Case 12.3 Hodgkin Lymphoma (HL), Staging, Monitoring Treatment Response and Follow-Up (Fig. 12.3)

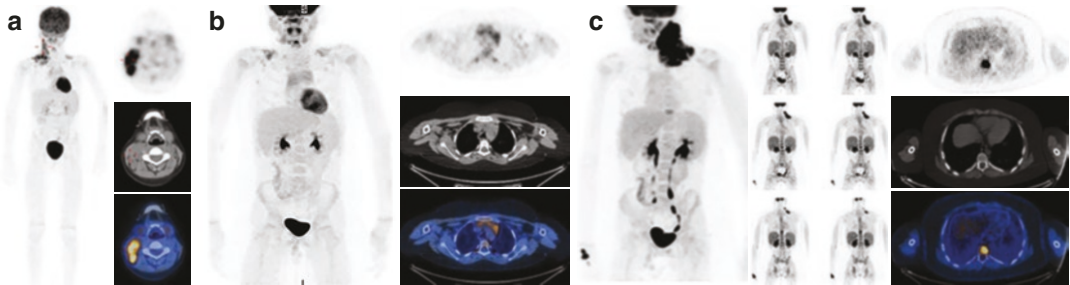


Fig. 12.3 History: A 7-year-old boy with newly diagnosed HL. Study report: At staging (a) FDG-PET MIP and selected transaxial PET, CT, and PET/CT slices at the level of the upper neck show intense abnormal tracer uptake in a nodal mass involving the neck and supra- and infra-clavicular regions on the right. Note also mild increased physiologic activity in bilateral infraclavicular sites of brown fat and in the thymus in the anterior mediastinum. There is no nodal hypermetabolism in the chest and no pulmonary nodules. There is no nodal hypermetabolism in the abdominal, retroperitoneal, or pelvic lymphatic chains. The spleen is normal in size and tracer avidity. There are no areas of abnormal uptake in the appendicular and axial skeleton. Impression: Supradiaphragmatic sites of nodal HL. The patient received treatment according to protocol and achieved a complete response. At the end of treatment (b): MIP and selected PET, CT, and transaxial PET/CT slices at the level of the upper mediastinum show that the supradiaphragmatic abnormal uptake foci in sites of HL have disappeared. There is mild-to-moderate tracer activity in an enlarged hyperplastic thymus and in sites of physiologic brown fat above the diaphragm. There is no nodal hypermetabolism in the neck and chest and in the abdominal,

retroperitoneal, or pelvic lymphatic chains. There are no pulmonary nodules. The spleen is normal in size and tracer avidity. There are no areas of abnormal uptake in the appendicular and axial skeleton. Impression: No evidence of active HL. Increased uptake in the thymus, consistent with post-treatment hyperplasia. The patient was followed up and re-evaluated 2 years later for suspicion of recurrence. At restaging (c): MIP (left), selected coronal PET slices (center) and transaxial PET, CT (with bone windows), and PET/CT slices at the level of the lower thorax (right) show new, intensely abnormal tracer uptake in significant lymphadenopathy in the left cervical, supra- and infra-clavicular regions. Note mild physiologic uptake in a hyperplastic thymus. There is no nodal hypermetabolism in the chest and in abdominal, retroperitoneal, or pelvic lymphatic chains. There is a new focal site of increased tracer uptake in the T9 vertebral body, with no corresponding lesion seen on CT. In addition, there is diffuse homogeneous increased activity throughout the skeleton. Impression: The findings are consistent with sites of nodal and skeletal recurrence of HL. Diffuse increased tracer activity in the skeleton, most probably reactive to increased hematopoiesis

**Case 12.4 Post-transplant
Lymphoproliferative Disorder (PTLD),
Transformation to Non-Hodgkin's
Lymphoma (NHL)–PET/MRI (Fig. 12.4)**

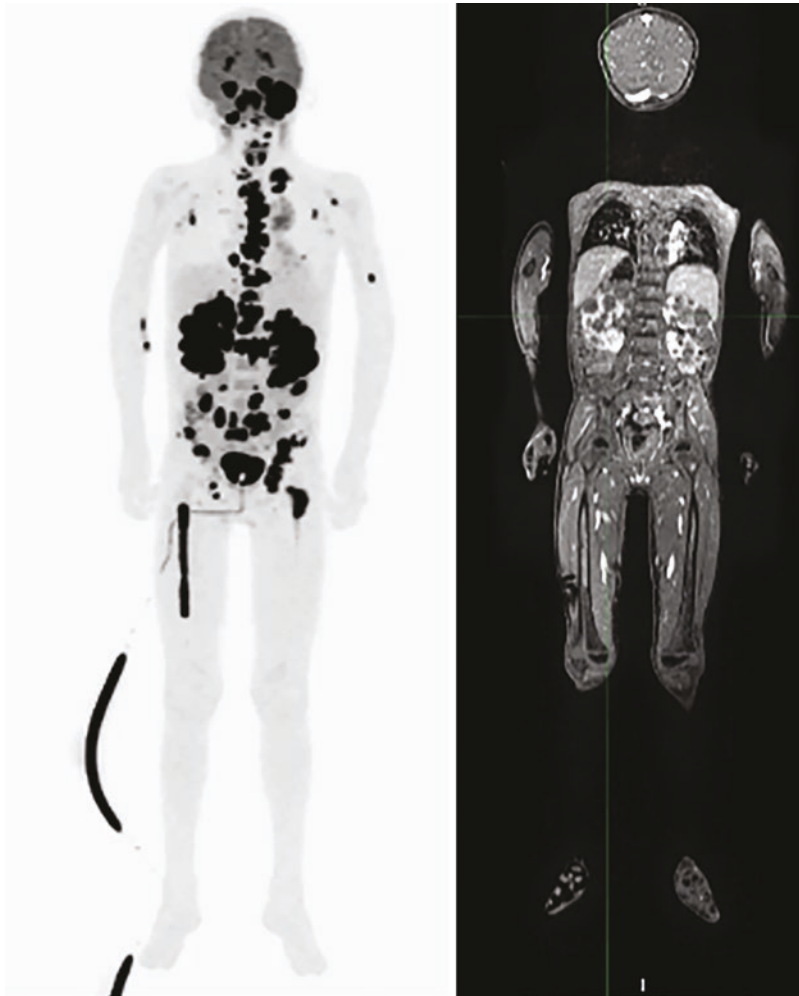


Fig. 12.4 History: A 7-year-old boy with known heterotaxy. Status after heart transplant in 2013, presented with a left neck mass. At clinical examination, he was found to have diffuse lymphadenopathy, small bowel intussusception, and kidney masses. The patient was referred with a suspicion of PTLD. PET/MRI was performed after administration of FDG and contrast for the MRI component. Study report: MIP images of FDG-PET and MRI demonstrate tracer activity in both maxillary sinuses, in a right costo-phrenic lymph node and in bilateral avid pulmonary nodules, mainly in a left apical pleural-based lesion. There is focal uptake in bowel in the right upper quadrant, due to small bowel-small bowel intussusception seen on prior CT. There is abnormal uptake in a conglomerate of left renal masses. There is no nodal hypermetabolism in the abdominal, retroperitoneal, or pelvic lymphatic chains. The spleen is absent, consistent with the history of

heterotaxy. There are multiple abnormal foci of tracer uptake in the skeleton. A soft tissue mass encompasses the left mandibular ramus. Additional foci of increased activity are seen in the mandible and maxilla bilaterally, the occiput, the left glenoid, the pelvic bones, the right femoral shaft, and the left femoral neck. Diffuse bony involvement includes multilevel vertebral bodies, some with soft tissue and epidural extension. There is increased uptake and enhancement along multiple nerve roots, such as the sacral nerves and left L2 nerve root. Impression: The findings are consistent with diffuse FDG-avid disease including bony involvement of the axial and appendicular skeleton, bilateral renal masses, lymphadenopathy above the diaphragm, bowel involvement, and lung lesions, suggesting PTLD with transformation to NHL, further confirmed by subsequent biopsy. Status after known heterotaxy and orthotopic heart transplant

Case 12.5 Osteosarcoma, Metastatic to Bone, Staging (Fig. 12.5)

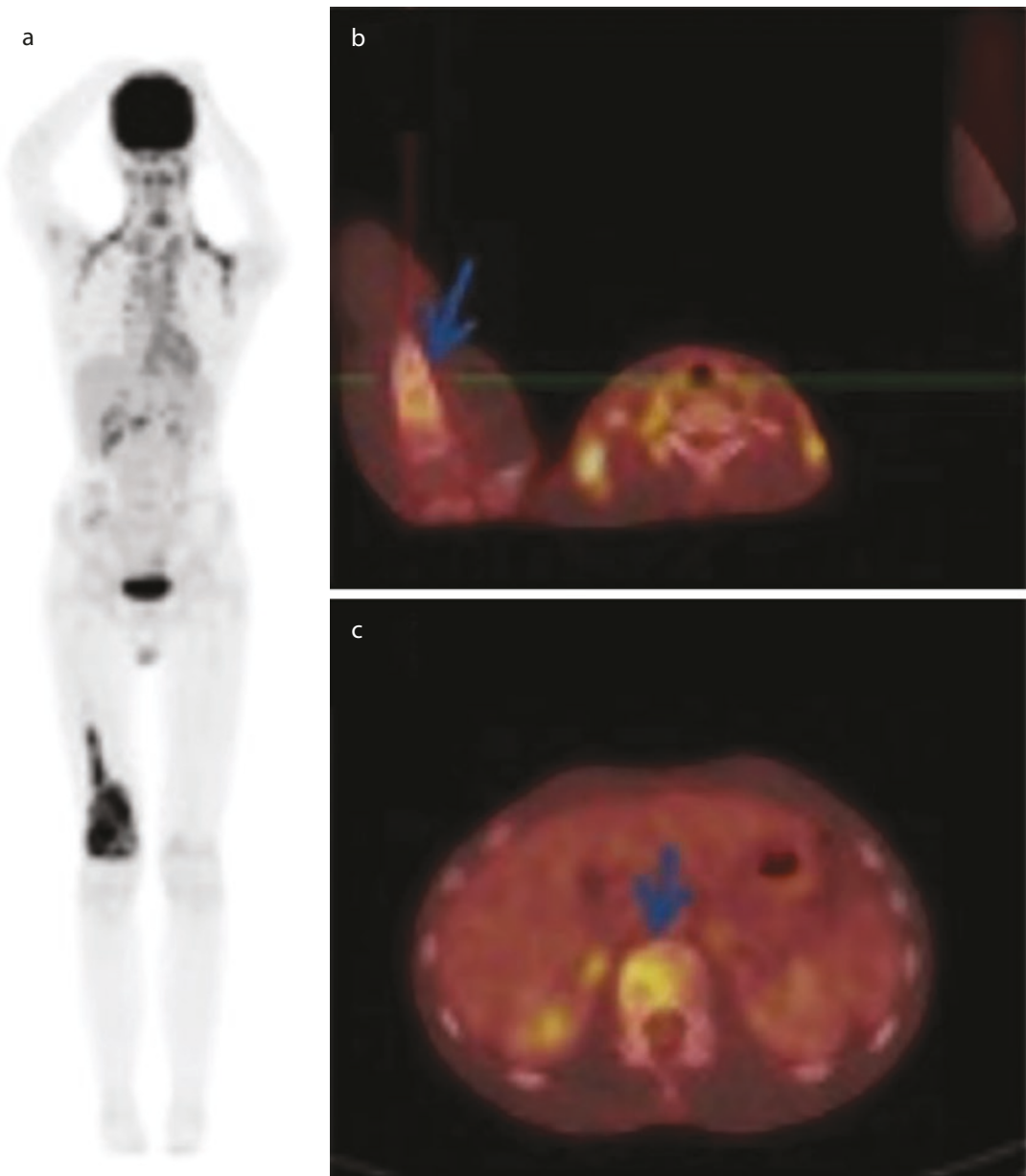


Fig. 12.5 History: A 14-year-old girl presented for evaluation of a destructive lesion in the right distal femur suggestive of a primary bone tumor. Study report: There is no nodal hypermetabolism in the head and neck. Note physiological cervical and axillary uptake in brown fat. There is no nodal hypermetabolism in the chest and no pulmonary nodules. There is no nodal hypermetabolism in abdominal, retroperitoneal, or pelvic lymphatic chains. The

spleen is normal in size and tracer avidity. There is intense tracer uptake in the known lesion in the distal right femur seen on the FDG-PET MIP image (a). Additional foci of moderately increased tracer uptake are seen in mixed, lytic-blastic bone lesions in the right proximal humerus (b, arrow) and L2 vertebral body (c, arrow). Impression: The findings are consistent with right femur osteosarcoma with skeletal metastases

Case 12.6 Metastatic Rhabdomyosarcoma (Fig. 12.6)

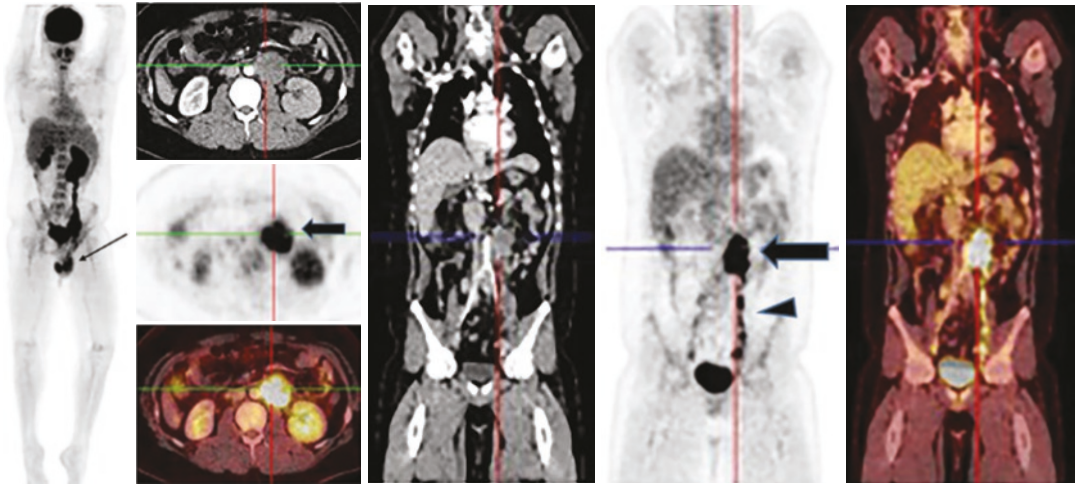


Fig. 12.6 History: A 14-year-old boy presented with a left testicular mass. FDG-PET/CT was performed for staging evaluation. Study report: MIP (left), transaxial (center) and coronal (right) CT, PET, and fused slices at the level of retroperitoneal lymphadenopathy demonstrate focal increased tracer activity in the left testicular mass (thin arrow), hypermetabolic left retroperitoneal paraaor-

tic lymphadenopathy, extending from the level of the left kidney (thick arrow and arrowhead) to just above the bladder. Impression: The findings are consistent with left testicular neoplasm with left retroperitoneal extensive metastatic lymphadenopathy. Biopsy diagnosed rhabdomyosarcoma

12.3 Neuroblastoma

Clinical Indications [11]

- Staging.
- Prognostic information based on scoring methods measuring disease extent.
- Assessment of response to treatment.
- Restaging of recurrence.
- Long-term surveillance.
- Imaging prior to treatment with radiolabelled tracers: ^{123}I -MIBG scan will determine whether a neuroblastoma is tracer-avid and treatment with ^{131}I -MIBG can be considered.

Correlative Imaging [37, 38]

- Neuroblastoma will often present as an abdominal mass and the US will be the initial imaging study. Characteristic calcification and location of disease may suggest the likelihood of neuroblastoma diagnosis.
- Bone scintigraphy is not routinely performed in a child presenting with suspected neuroblastoma since MIBG scintigraphy and PET imaging have replaced this test. However, a child presenting with bone pain or limp may have initial imaging with a bone scan.
- Bone scintigraphy in a patient with suspected neuroblastoma can show typical abnormal, often symmetrical metaphyseal activity, focal bony lesions in the axial and appendicular skeleton as well as soft tissue uptake in a, mainly abdominal, mass (see Case 12.14, and Fig. 12.15).
- Plain radiographs can show no abnormalities in cases with skeletal involvement of neuroblastoma.
- MRI is the most common study performed to evaluate a mass in the chest, abdomen, and/or pelvis, in a child with neuroblastoma. It is mandatory when epidural and intracranial disease is suspected.
- CT scans may also be used for imaging evaluation of chest, abdomen, and pelvic disease suspected to be neuroblastoma. It is not adequate as the single cross-sectional anatomic

imaging modality when epidural or intracranial disease is suspected.

MIBG Scintigraphy of Neuroblastoma

Specific Study Interpretation Criteria (See also Box 12.2—Imaging with MIBG)

- Pathological tracer uptake is found in the primary tumor and in metastases in lymph nodes, liver, bone, bone marrow, and rarely, skin, lungs, and brain.

MIBG Scoring Systems [39]

- Provides a semiquantitative assessment of initial disease burden and response to therapy.
- It is used for treatment tailoring and for prognosis.
- Two validated scoring systems are in use:
 - The Curie Score (Children’s Oncology Group—COG) divides the skeleton into 9 compartments and a 10th compartment for the soft tissues. The uptake score for each compartment ranges from 0 to 3 [40].
 - The SIOPEN score (International Society of Paediatric Oncology Europe Neuroblastoma), only scores skeletal disease. The skeleton is divided into 12 segments. The uptake score for each segment reflects the disease extent in that segment and ranges from 0 to 6 [41].

Red Flags [14]

- Careful drug history should be obtained before imaging. Numerous drugs interfere with the uptake or retention of MIBG and should be discontinued for approximately 4 biological half-lives. A detailed list of interfering drugs, most of them rarely used in children, can be found in Appendix 1 of the EANM guidelines [11]. The main drugs to be withdrawn in children are those used for symptomatic treat-

ment of asthma and of upper respiratory tract infections (decongestants), and occasional antihypertensive drugs.

- Thyroid blockage medication is required to prevent unnecessary irradiation of the thyroid gland by free radioiodine. Sedation, especially important for SPECT/CT, may be required because most children undergoing MIBG scintigraphy are young, and acquisition takes 60–90 min. In some occasions, feeding and bundling the infant prior to scan is all that is required to keep the child immobile.
- Slow administration of the tracer reduces the likelihood of adverse reactions such as hypertension, nausea, vomiting, and pallor that may occasionally occur.
- Children should be monitored during, and for a short time after, MIBG injection.
- The most appropriate collimator type for ^{123}I -MIBG imaging varies among different manufacturers and should be decided based on the equipment available in each department.
- In young children, multiple spot views should be used because of higher count density and improved spatial resolution. Multiple views obtained for the skull (anterior, posterior, left, and right lateral views) improve detection of orbital and skull base lesions.
- A full bladder can conceal pelvic lesions. Post-void images, SPECT, and/or SPECT/CT of the pelvis and less commonly, bladder catheterization can be employed.

Take Home Messages [14]

- Primary tumors most commonly originate from the adrenal gland or from the sympathetic ganglia, along the abdominal, thoracic, and rarely cervical spine.
- MIBG is an iodinated analogue of guanidine, structurally similar to norepinephrine (NE). It shares the same transport pathway as NE via the cell membrane NE transporter system. In the cytoplasmic compartment, MIBG is stored in the neurosecretory granules.
- For functional imaging assessment of neuroblastoma, ^{123}I -MIBG is considered a first-line

test. It is the current standard due to appropriate physical characteristics for the best image quality and dosimetry.

- ^{131}I -MIBG should not be used for diagnostic purposes due to poor image quality and higher radiation exposure.
- About 10% of neuroblastomas do not accumulate MIBG.
- Any MIBG uptake in the skeleton indicates metastatic disease.
- SPECT/CT is of particular value for:
- Differential diagnosis of heterogeneous hepatic tracer uptake, a known physiologic pattern vs. metastatic involvement.
- To distinguish intracranial from skull lesions. Lesions involving the calvarium are on rare occasions due to cerebral metastases.
- Distinction between cortical bone and bone marrow metastases.
- Discrepancy in MIBG uptake between the primary tumor and metastases may be due to:
 - Biological heterogeneity in populations of tumor cells can alter their MIBG avidity.
 - Changes occur during the course of the disease course.
 - MIBG avidity of relapsed disease might differ from the initial disease.
 - After treatment, uptake in residual tumor deposits may persist due to differentiation of the tumor to mature MIBG-avid ganglioneuroma.
 - MIBG imaging plays a theranostic role in the assessment of neuroblastoma.
 - Alternative imaging of neuroblastoma with PET tracers can be considered.

PET Imaging of Neuroblastoma (see also Box 12.1, Box 12.3, and Box 12.4)

Clinical Indications [42, 43]

- Alternative metabolic imaging in cases of MIBG-negative or weakly positive tumor.
- When radiologic imaging modalities show more disease than MIBG scintigraphy.
- Advantages of PET imaging of neuroblastoma include:

- One-day appointment
- No need for iodine blockage
- Faster scan
- Lesser need for anesthesia
- Improved lesion detectability
- Quantitation of tracer uptake

FDOPA [44–46] (*See also* Box 12.3)

- FDOPA uptake is relatively specific for NETs including neuroblastoma. When available, it is considered the preferred PET alternative to ^{123}I -MIBG.

Red Flags

- In adults, carbidopa reduces physiologic uptake in peripancreatic region and increases uptake in lesions. However, there is no consensus regarding the use of carbidopa in children.
- Avoid misinterpretations by performing late imaging after ambulation/hydration/diuretic administration.

Take Home Messages [47]

- DOPA is present in the nervous system as a precursor of dopamine and FDOPA PET imaging tracks the metabolism of catecholamines.
- Neuroblastoma FDOPA PET imaging provides a sensitive and specific assessment of the disease status. While being a relatively specific tracer for NETs other indications are also known.
- Small-scale studies comparing FDOPA with ^{123}I -MIBG in children show a higher sensitivity of the former tracer and superior detectability of small metastases in bones, soft tissues, and bone marrow.

FDG [5] (*see also* Box 12.1)

- Advantages:
 - Uptake is proportional to the degree of malignancy.

- Prognostic value with higher FDG uptake at diagnosis is associated with poorer prognosis.
- It can differentiate between residual active tumor and benign ganglioneuromas which maintain MIBG avidity but are typically FDG negative.

- Limitations:

- Lack of specificity, mainly for assessing the presence of bone marrow involvement, a very common location for neuroblastoma metastases and also a site of physiologic FDG uptake.
- Cranial vault lesions may be difficult to detect on FDG imaging due to the adjacent high brain activity.

^{68}Ga -PEPTIDES [15, 48, 49] (*see also* Box 12.4)

Clinical Indication

- ^{68}Ga -peptides target SSTR which are commonly expressed in neuroblastoma cells.
- To select suitable patients for theranostics using peptide receptor radionuclide therapy (PPRT).

Red Flags

- Poorly differentiated tumors have a low affinity for the tracer.
- Inflammatory processes such as reactive lymph nodes or post-radiotherapy changes may show some degree of tracer activity, usually of mild intensity, due to the expression of SSTRs in activated lymphocytes.
- Further validation is required prior to increasing the utilization of this modality in routine clinical practice.
- SSTR imaging to determine whether a NET is receptor positive. Peptide receptor radionuclide therapy (PRRT) such as ^{177}Lu -DOTA-octreotate is, in pediatric patients, still investigational.

Take Home Messages

- Pathological uptake in neuroblastoma is typically intense SUVs.
- Somatostatin receptor imaging of neuroblastoma is a sensitive, second-line PET alternative to ^{123}I -MIBG with a potential for theranostic application.
- All these tracers target SSTRs.

- They have rapid clearance from the blood and renal excretion. Maximum tumor activity is reached at 70 ± 20 min.

Relevant Case Examples

Case 12.7 Metastatic Neuroblastoma—MIBG Scintigraphy (Fig. 12.7)

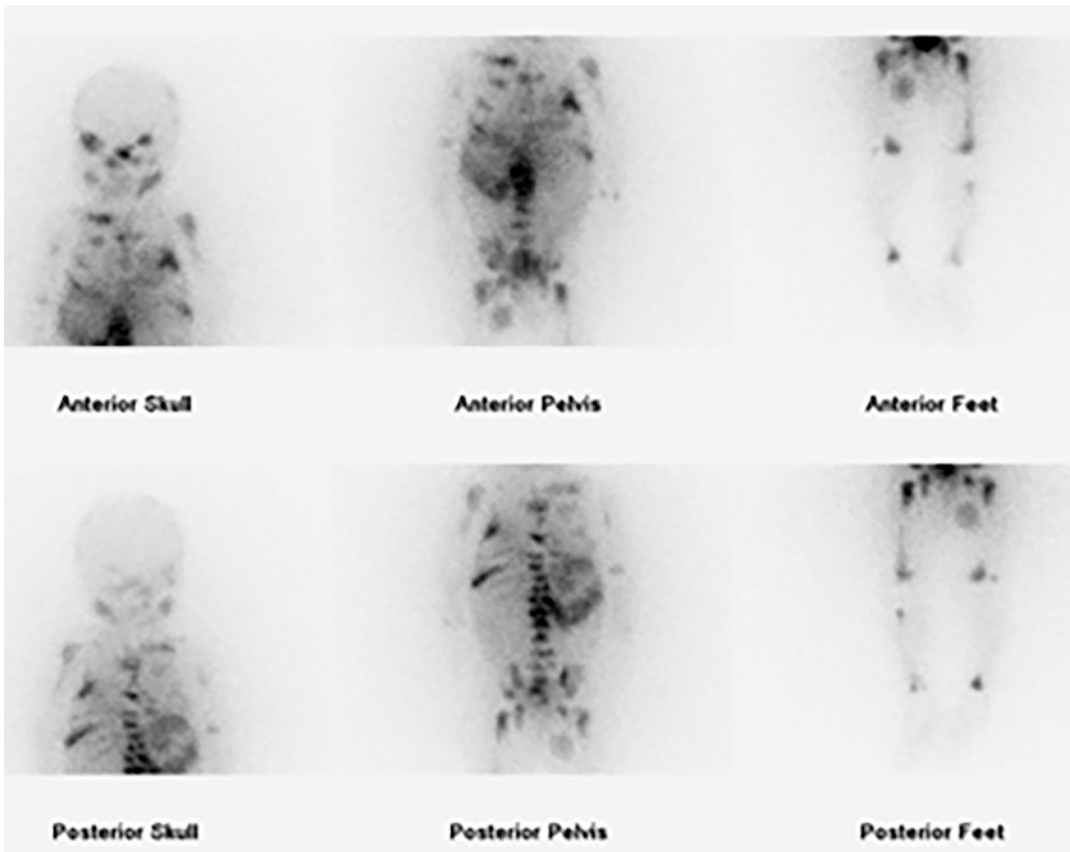


Fig. 12.7 History: A 16-month-old boy presented with multiple soft tissue masses over the right eye and the right thigh, and an additional palpable mass in the abdomen. Biopsy of the right thigh mass and of the bone marrow diagnosed neuroblastoma. Study report: MIBG scintigraphy, anterior and posterior planar spot views of the whole body, demonstrate foci of abnormally increased tracer

uptake involving the known soft tissue masses in the roof of the right orbit, in the right upper abdomen (with a cold, photopenic, central area, most probably necrosis) and the upper right thigh. There are also multiple foci of increased tracer uptake in the skeleton, in the left mandible, ribs, and vertebrae. Impression: The findings are consistent with metastatic neuroblastoma

Case 12.8 Metastatic Neuroblastoma, Response to Treatment—MIBG Scintigraphy (Figs. 12.8 and 12.9)

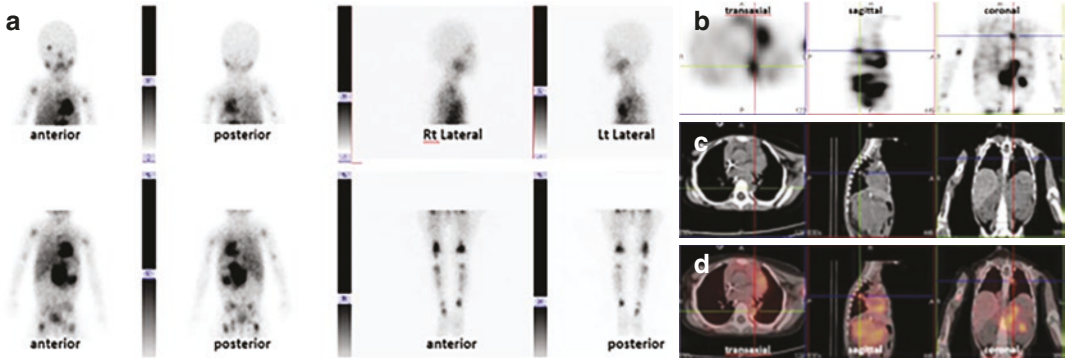


Fig. 12.8 History: An 18-month-old infant girl presented with a large abdominal mass suspected of neuroblastoma. A baseline MIBG scan was obtained for initial staging. Study report: Planar spot images of the whole body (a) show intense tracer uptake in the abdominal mass, as well as in multiple skeletal metastases in the skull, upper limbs, pelvis, and lower limbs. SPECT, low dose CT and SPECT/

CT transaxial, sagittal, and coronal slices (b–d) show a left paravertebral, metastatic mediastinal mass (cross hair) that was not evident on planar images. Impression: The findings suggest metastatic neuroblastoma, further confirmed by biopsy of the abdominal mass. The patient started induction chemotherapy

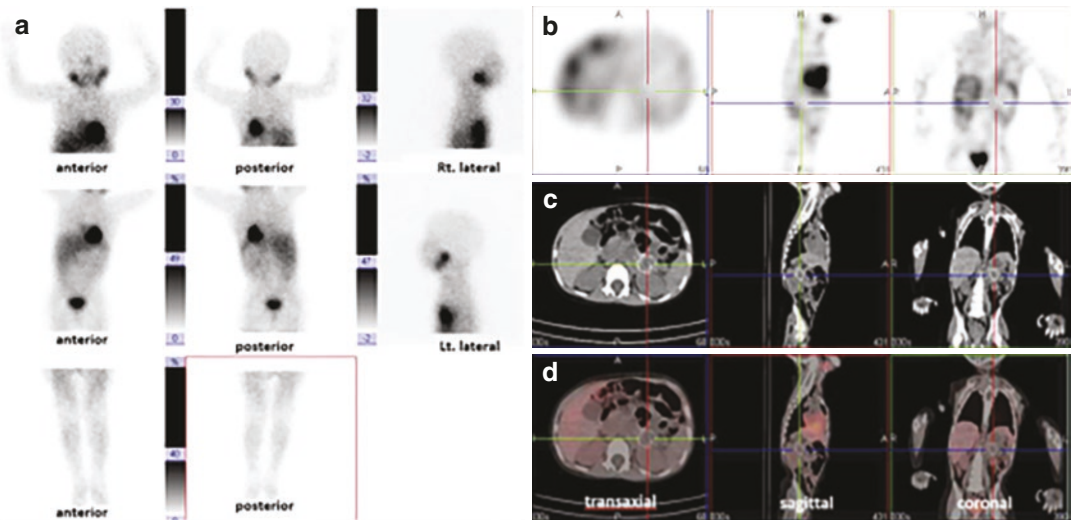
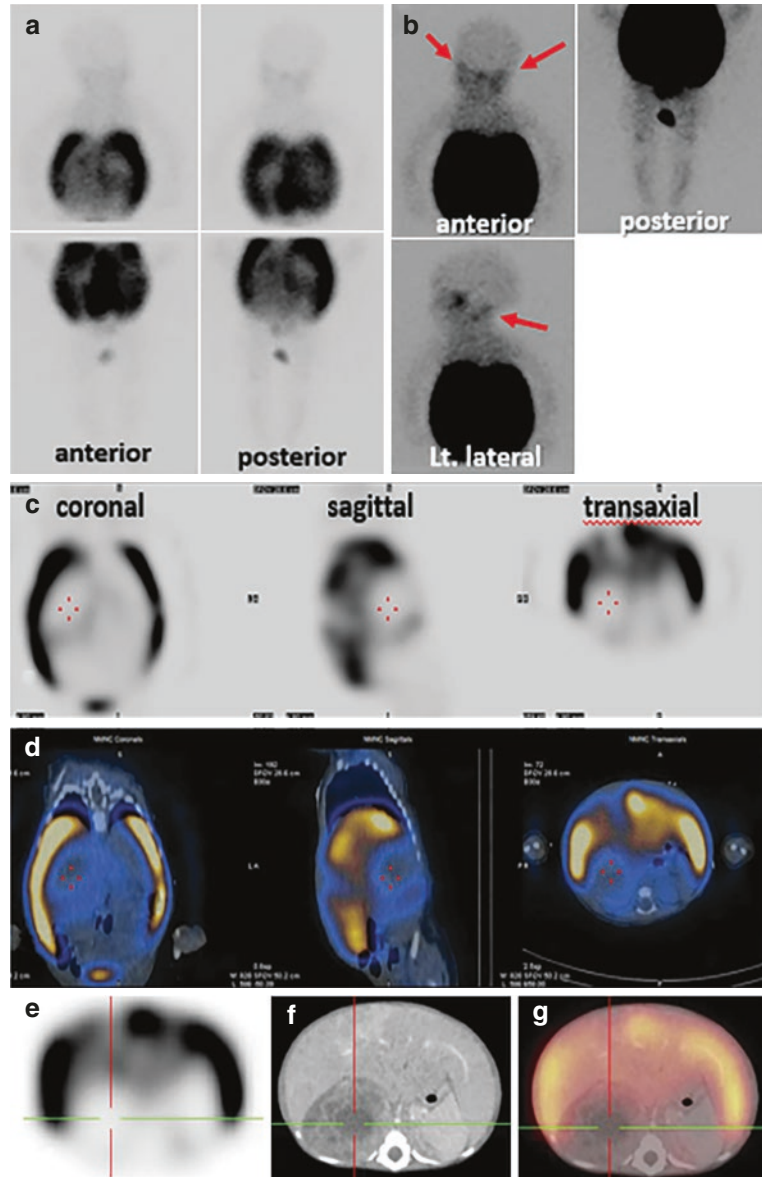


Fig. 12.9 A follow-up ¹²³I-MIBG scan was obtained 2 months after the start of treatment according to the therapy protocol. Study report: MIBG scintigraphy, anterior, and posterior planar spot views of the whole body, (a) show normal tracer distribution with a resolution of the uptake in the abdominal tumor and in the metastatic sites.

Transaxial, sagittal, and coronal SPECT, CT, and SPECT/CT slices (b–d) demonstrate that the size of the abdominal tumor has significantly decreased. The crosshair is positioned over a calcified portion of the residual tumor and shows no tracer uptake. Impression: The findings indicate a complete metabolic response

Case 12.9 Metastatic Neuroblastoma, Heterogeneous Uptake on MIBG Scintigraphy (Fig. 12.10)

Fig. 12.10 History: A 2-month-old girl presented with a large right-sided abdominal neuroblastoma and massive enlargement of the liver. MIBG SPECT/CT was obtained for initial staging. Study report: scintigraphy, anterior and posterior spot views of the whole body (a) shows intense tracer uptake in a huge liver occupying both sides of the abdomen. Tracer activity in the rest of the body is faint. Using manipulation of the image gray scale (b) physiological tracer localization is identified in the orbits, skull base (arrows), and lower limbs. Transaxial and sagittal SPECT (c) and fused SPECT/CT slices (d) show intense tracer uptake in an enlarged liver occupying both sides of the abdomen. There is no appreciable MIBG uptake in the primary tumor in the right upper abdomen (crosshair). SPECT co-registered to an external diagnostic, contrast-enhanced CT to better delineate the primary tumor (e–g) shows no MIBG uptake in a large abdominal tumor. Impression: The findings are consistent with a non-MIBG-avid abdominal neuroblastoma with MIBG-avid metastases to liver and bone marrow. The difference in MIBG avidity between the primary tumor and the distant metastases reflects the biological heterogeneity of neuroblastoma cell populations



Case 12.10 Neuroblastoma, Tumor Progression, PET/CT with FDOPA (Fig. 12.11)

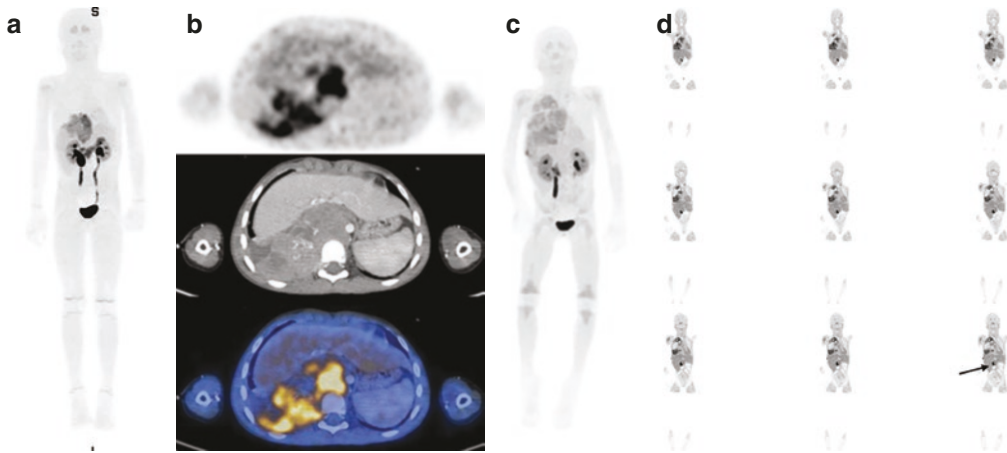
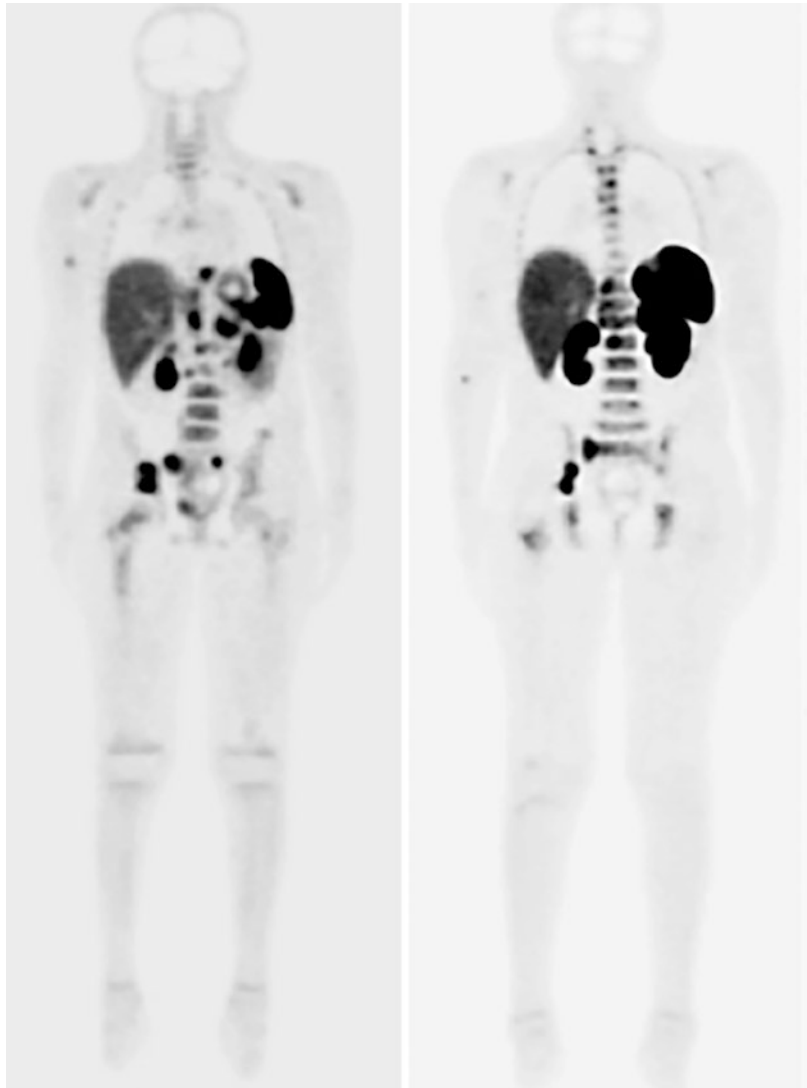


Fig. 12.11 History: A 5-year-old boy presenting with a thoracoabdominal mass was referred with the suspicion of neuroblastoma. Study report: At diagnosis MIP (a) and selected transaxial PET, CT, and PET/CT slices at the level of the lower thorax/upper abdomen (b) show an area of inhomogeneous abnormal tracer uptake (SUVmax up to 6.4) in a heterogeneous mass, $7 \times 10 \times 10$ cm in size, located right paravertebral to the lower thoracic spine, most probably involving the right foramina of T10. There is no increased activity in lymph nodes in the neck and chest and in the abdominal, retroperitoneal, or pelvic lymphatic chains. There are no pulmonary nodules. The spleen is normal in size and tracer avidity. There are no areas of abnormal uptake in the appendicular and axial skeleton. Impression: The findings suggest the diagnosis

of neuroblastoma with suspected involvement of the right foramina of T10. The diagnosis of intermediate-risk neuroblastoma was confirmed by pathology. Laminectomy of T7–T10 with partial surgical removal of the tumor was performed and protocol treatment was started. At 2 months post-surgery a 2nd FDOPA PET/CT study was performed prior to the institution of a new treatment line. MIP (c) and selected coronal PET slices (d) demonstrate intense abnormal tracer uptake in new right supraclavicular lymphadenopathy, in a conglomerate of pleural nodules in the right hemithorax that involve the mid- and lower mediastinum and the chest wall muscles and in right para-aortic lymph nodes (arrow). Impression: The findings demonstrate significant tumor progression

Case 12.11 Metastatic Neuroblastoma, PET/CT with ^{68}Ga -DOTATATE PET/CT (Fig. 12.12)

Fig. 12.12 History: An 8-year-old girl with refractory stage 4 neuroblastoma was referred to PET/CT to determine suitability for ^{177}Lu -DOTATATE therapy. Study report: PET MIP, anterior, and posterior views, show multiple areas of abnormal tracer uptake in the primary tumor in the upper abdomen and in skeletal metastases involving vertebrae, the pelvis, and proximal femuri. Impression: The findings are consistent with metastatic neuroblastoma with SSTRs, a suitable candidate to PRRT



12.4 Other Neuroendocrine Tumors

⁶⁸Ga-PEPTIDE IMAGING OF NETS (see also Box 12.4—Imaging with ⁶⁸Ga-peptides)

Clinical Indications [15]

- Localization and characterization of NETs with the expression of high density of SSTR such as succinate dehydrogenase (SDHx)-mutated NETs and head and neck PGL when ¹⁸F-FDG-PET is negative.
- Detection of occult NETs in cases of metastatic tumors with unknown primary or if high serum tumor markers are found.
- Characterization of a bronchial tumor mass.
- In the theranostic setting, when PRRT is considered.

Red Flags [50]

- Brown fat visualization is not a common problem in ⁶⁸Ga-peptide imaging in NETs.

Take Home Message

- In well-differentiated NETs, ⁶⁸Ga-peptides PET imaging has a higher detection rate as compared to FDG imaging which may play a complementary role, especially in cases of poorly differentiated tumors known to show high FDG avidity.
- ⁶⁸Ga-peptides PET may evolve as a preferred imaging modality for disease surveillance in certain cancer predisposition or premalignancy syndromes (e.g., von Hippel Lindau disease).

FDOPA IMAGING OF NETS (*See also* Box 12.3—Imaging with FDOPA)

Clinical Indications [51, 52]

- NETs with absent SSTR expression, for (re) staging and monitoring response to treatment.
- Adrenal pheochromocytoma, sporadic or related to cancer predisposition syndromes.
- Congenital hyperinsulinism, to identify focal forms in the pancreas that can be resected [53].

Red Flags

- Inflammatory processes such as reactive lymph nodes or post-radiotherapy changes may show tracer activity.
- SSTR imaging to determine whether a NET is receptor positive. Peptide receptor radionuclide therapy (PRRT) such as ¹⁷⁷Lu-DOTA-octreotate is, in pediatric patients, still investigational.

Take Home Message

- FDOPA PET imaging is more specific in cases of neuroblastoma and insulinoma as compared with FDG and ⁶⁸Ga-peptides.
- Advantages of NET PET imaging (over NET SPECT imaging):
 - Earlier and shorter acquisition time
 - Improved patient comfort
 - Improved spatial resolution
 - Less radiation exposure

Representative Case Examples

Case 12.12 Paraganglioma (PGL), ⁶⁸Ga-DOTATE PET/CT (Fig. 12.13)

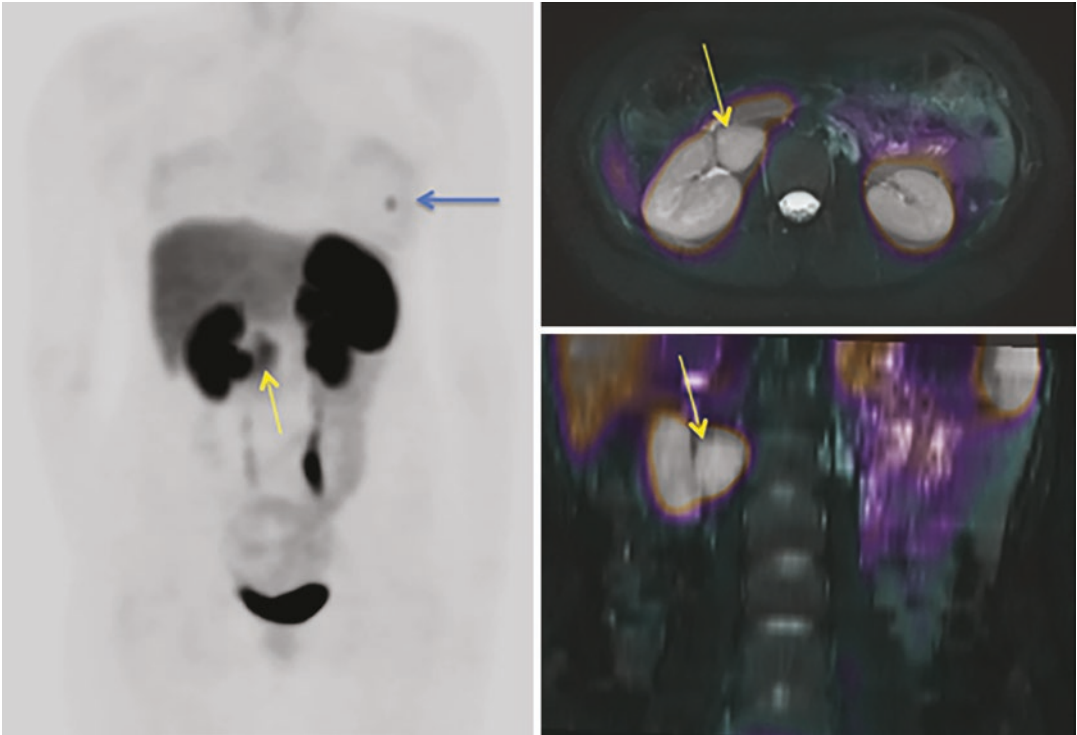


Fig. 12.13 History: A 9-year-old girl presented with hypertension and headaches and was diagnosed with a right lumbar paravertebral PGL with a SDH gene line mutation. The tumor was resected and hypertension and symptoms improved. Four years later, at the age of 13 years, the patient presented again with hypertension. MRI showed recurrence of the mass in the right paravertebral region. PET/CT was performed for restaging of the recurrence. Study report: MIP (left) and selected transaxial (right top) and coronal (right bottom) PET/CT slices at the level of the mid-abdomen show increased focal tracer

uptake in the right paravertebral mass (yellow arrow) as well as in a metastatic focus in the left 6th rib (blue arrow). There is no increased activity in lymph nodes in the neck and chest and no pulmonary nodules. There are no additional areas of abnormal uptake in the appendicular and axial skeleton. Impression: The findings are consistent with recurrent PGL metastatic to bone. Both sites were resected, however, a follow-up scan performed 6 months later showed tumor progression with multiple bone metastases. The patient was treated with ¹⁷⁷Lu- DOTATATE and remained stable for 2 years

**Case 12.13 Pheochromocytoma—FDG-PET/
CT (Fig. 12.14)**

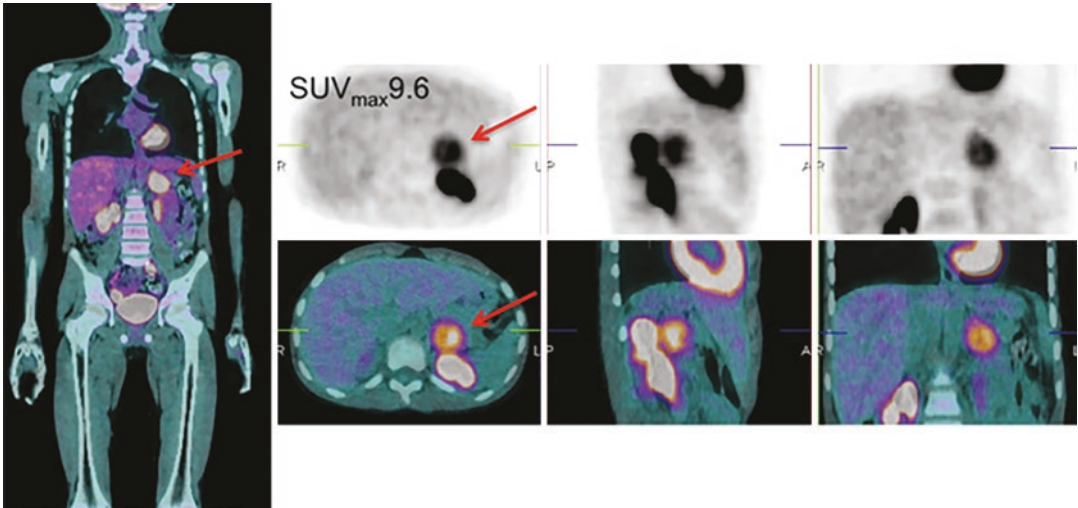


Fig. 12.14 History: An 11-year-old boy presented with hypertension. CT scan showed a left adrenal mass. ^{123}I -MIBG was negative (not shown). Study report: FDG-PET/CT shows abnormal uptake in the left adrenal mass (arrow) on transaxial, sagittal, and coronal PET (top right) and CT (bottom right) slices and coronal CT image of torso. There is no nodal hypermetabolism. There is no nodal hypermetabolism in the neck and chest and in the

abdominal, retroperitoneal, or pelvic lymphatic chains. There are no pulmonary nodules. The spleen is normal in size and tracer avidity. There are no areas of abnormal uptake in the appendicular and axial skeleton. Impression: The findings are suggestive of malignancy with no evidence of metastatic disease. Biopsy diagnosed pheochromocytoma

12.5 Musculo-Skeletal Malignancies (see also Box 12.5)

Clinical Indications [21, 23, 54–56]

- To identify and localize bone and bone marrow metastases in order to determine the extent of disease in patients with known malignancies.
- To assess primary bone and ST tumors such as osteosarcoma, Ewing sarcoma, and rhabdosarcoma.

Correlative Imaging

- In the presence of specific symptoms, plain radiographs are followed as a rule by MRI, the first choice investigation in most children with bone tumors.

Red Flags

- If MRI is not readily available or the child needs sedation or general anesthesia, bone scintigraphy and, recently in some centers, bone PET/CT are the next choice.
- For multiple spot views of the whole body start with the pelvis when the bladder is empty.
- It is still debated whether SPECT should be routinely performed even if planar scan is unremarkable or only for better characterization of an abnormality detected on planar imaging.
- When performing SPECT/CT the FOV of the CT should be shortened to include only the

region of the abnormality seen on SPECT to reduce radiation exposure.

- The CT component of a bone SPECT/CT can be acquired as a pediatric low-dose CT for localization and attenuation correction or as a diagnostic CT. Many skeletal lesions are adequately evaluated even with low-dose CT parameters.

Take Home Messages

- Increased tracer uptake, due to locally increased blood flow or calcium depositions, indicates an alteration in bone metabolism caused by increased new bone formation (osteoid) due to higher availability of binding sites, but also related to local or regional hyperemia.
- Bone marrow lesions tend to have a more diffuse pattern along a portion of a bone whereas cortical bone lesions are typically focal.
- With the dissemination of FDG-PET imaging which is the method of choice in oncology, most centers use this modality as the main scintigraphic study for malignancies even when they are limited to bone. Skeletal scintigraphy is used only occasionally and thus the significant decrease in its use in children with cancer.
- NaF PET imaging is becoming the preferred alternative for imaging of the skeleton due to the tracer's rapid localization and rapid clearance from the blood.

Representative Case Examples

Case 12.14 Metastatic Neuroblastoma, Bone Scintigraphy

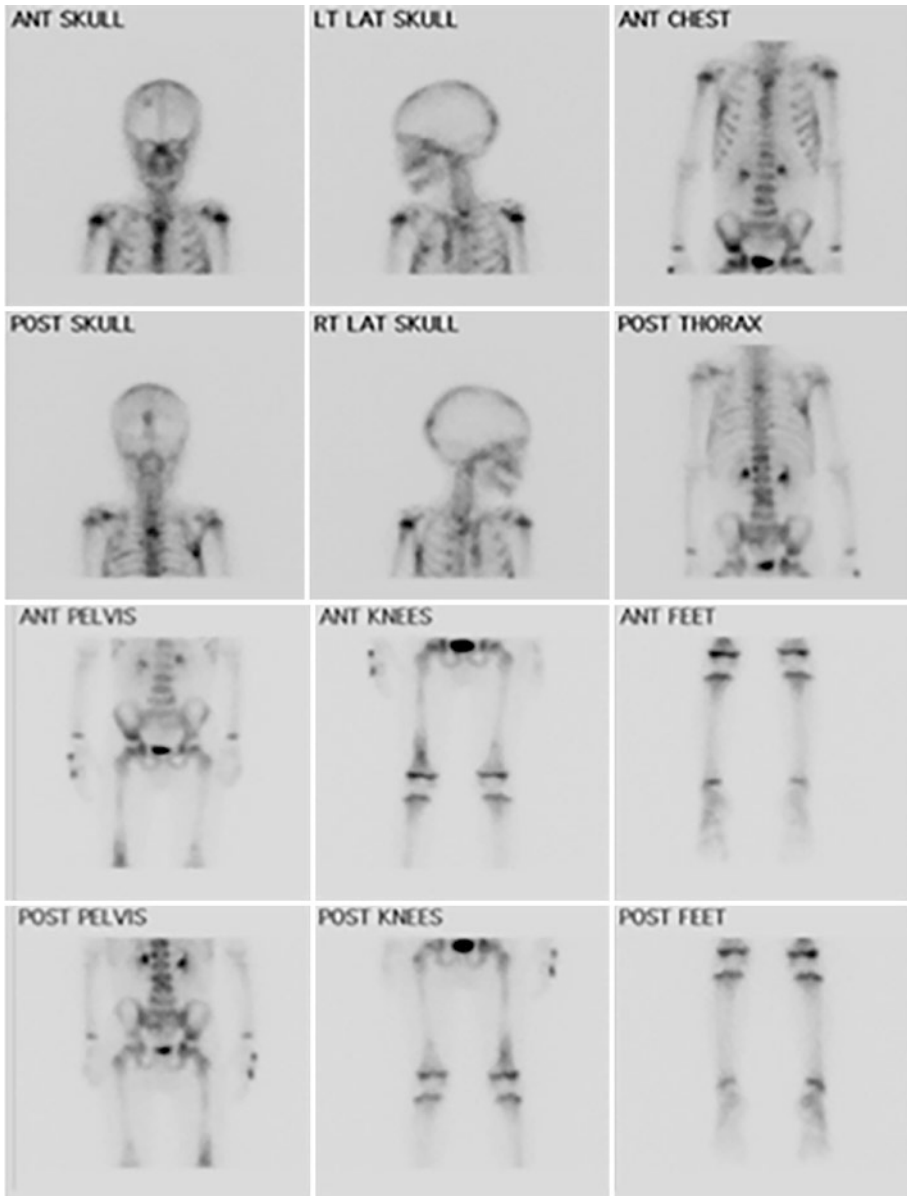


Fig. 12.15 History: A 5-year-old boy presented with right-sided limp. Clinical examination was normal. Plain radiographs of his pelvis and lower limbs were normal. Lab tests including ESR and CRP were mildly elevated. Study report: Bone scintigraphy, anterior and posterior planar spot views of the whole body, demonstrate multiple focal areas of increased tracer uptake in the skull, right proximal humerus, both scapulae, upper and lower tho-

racic and lumbar vertebrae, right acetabulum and distal femora (right more than left). Note asymmetrical metaphyseal activity specifically in the distal femora. Impression: The findings are consistent with neuroblastoma metastatic to bone. Abdominal US revealed a mass in the right adrenal. Tissue sampling diagnosis was stage IV neuroblastoma. Total body MIBG scintigraphy showed tracer uptake in the primary tumor and metastatic bone lesions

Case 12.15 Ewing Sarcoma, Staging, Bone Scintigraphy (Fig. 12.16)

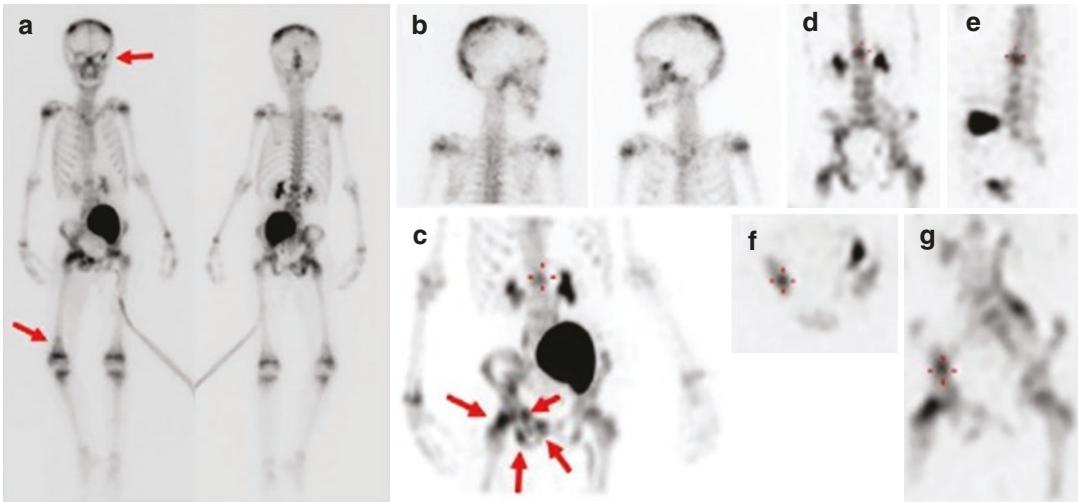


Fig. 12.16 History: An 8-year-old boy presented with a large pelvic mass. Histopathology diagnosed Ewing's sarcoma. Bone scintigraphy was performed for staging. Study report: Anterior and posterior whole body (a) and lateral spot views of the skull (b) show marked displacement of the urinary bladder to the left upper pelvis due to the known large tumor. Activity is noted in a urinary catheter to the left side of the body. Skeletal lesions are noted in the parietal and occipital skull, left orbit (arrow), L1,

acetabulum, the right pelvis involving the superior pubic ramus, ischium, and ilium, as well as in the proximal and distal (arrow) left femur. Coronal (d) and sagittal (e) SPECT slices show the L1 lesion (crosshairs). Transaxial (f) and coronal (g) slices show a lesion in the internal pelvic rim. MIP image (c) provides an overview of the pelvic and lumbar lesions (arrows). Impression: The findings suggest stage 4 pelvic Ewing's sarcoma with multiple skeletal metastases

Case 12.16 Metastatic Osteosarcoma, Bone Scintigraphy (Fig. 12.17)

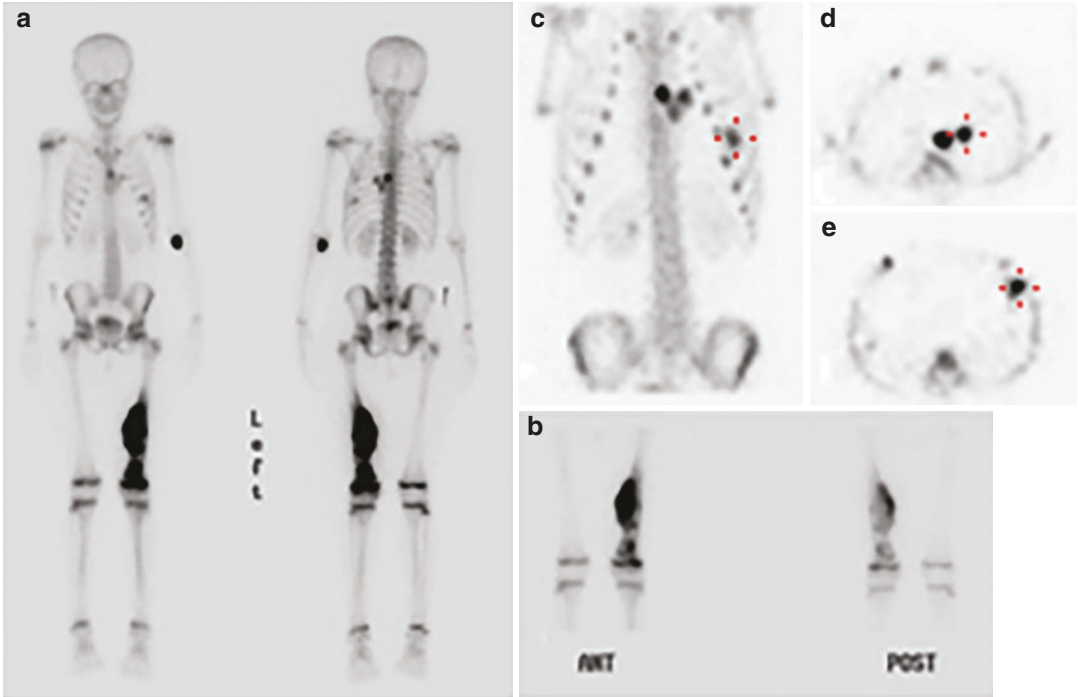


Fig. 12.17 History: An 8-year-old girl with left femoral osteosarcoma underwent bone scintigraphy for staging. Study report: Anterior and posterior whole body (a) and spot views (b) of the thighs show intense tracer uptake in the known primary tumor in the left mid-thigh. A “skip” lesion is seen in the distal left femur, better appreciated on the spot views (b). MIP (c) and transaxial slices (d, e)

from the SPECT of the thorax show several lesions in the left chest, localized to the posterior mediastinum and lung parenchyma. Impression: The findings are consistent with metastatic stage 4 osteosarcoma of the left femur with a skip lesion in the distal left femur and additional bone-forming metastases in the ST of the left hemithorax

Case 12.17 Osteosarcoma, NaF PET/CT
(Fig. 12.18)

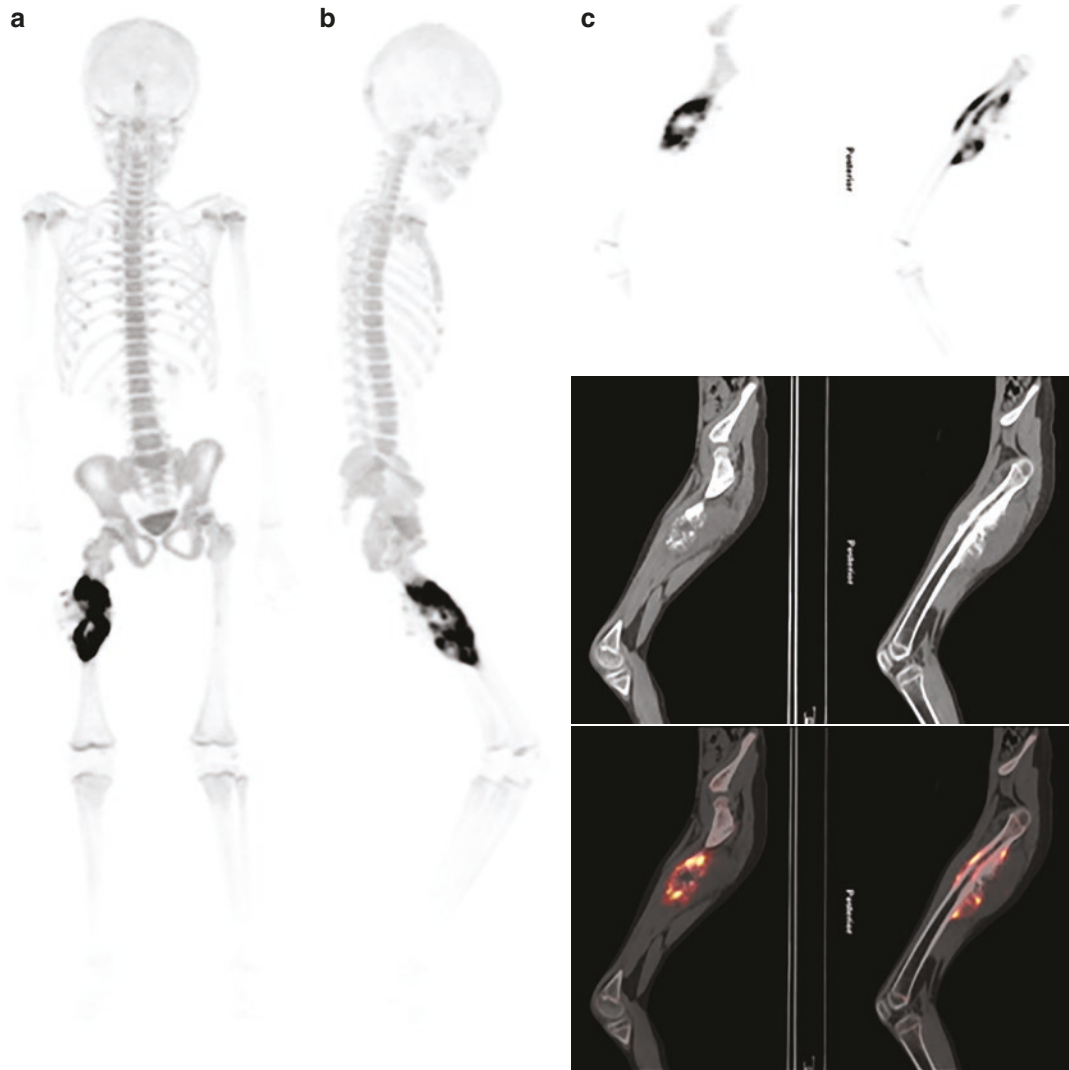


Fig. 12.18 History: An 8-year-old girl with chondroblastic osteosarcoma of the right femur performed NaF PET/CT for staging. Study report: Anterior (a) and lateral (b) MIP projections and sagittal PET, CT, and PET/CT slices at the level of the thigh (c) show inhomogeneous increase

tracer uptake in a destructive lesion in the mid-shaft of the right femur. No other skeletal lesions are seen. Impression: The findings demonstrate the primary osteosarcoma in the right femur with no evidence of metastatic spread

Case 12.18 Langerhans Cell Histiocytosis, NaF PET/CT (Fig. 12.19)

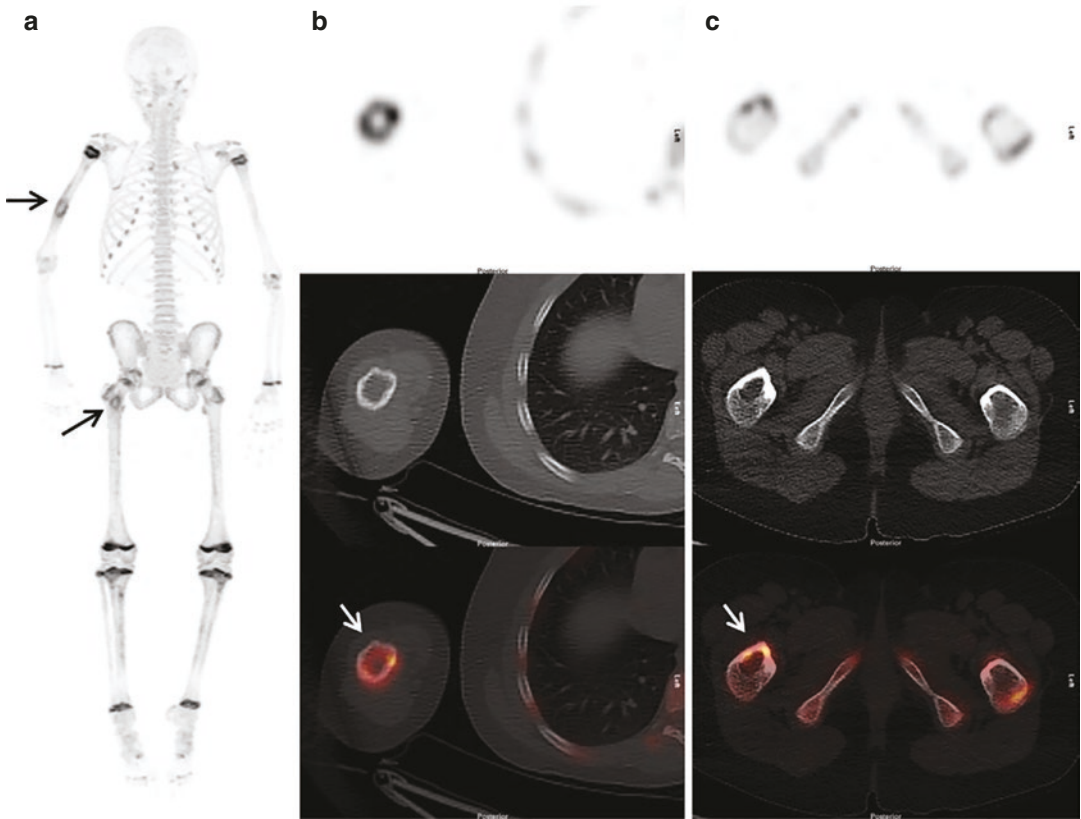


Fig. 12.19 History: A 11-year-old girl complains of right hip pain for 2 months and was referred to NaF PET/CT for further evaluation. Study report: Anterior MIP (a) and selected transaxial PET, CT, and PET/CT slices at the level of the mid-thorax (b) and lower pelvis (c) show two foci of inhomogeneous increased tracer activity localized

at the distal one-third of the right humeral shaft and the trochanteric region of the right femur, with corresponding lytic lesions on CT images (arrows). Impression: The findings are consistent with aggressive osteoblastic bone lesions in the right humerus and proximal right femur. Biopsy diagnosed Langerhans cell histiocytosis

References

1. Treves ST, et al. 2016 update of the North American consensus guidelines for pediatric administered radiopharmaceutical activities. *J Nucl Med.* 2016;57(12):15N–8N.
2. Lassmann M, Treves ST. Paediatric radiopharmaceutical administration: harmonization of the 2007 EANM paediatric dosage card (version 1.5.2008) and the 2010 North American consensus guidelines. *Eur J Nucl Med Mol Imaging.* 2014;41(5):1036–41.
3. Alessio AM, et al. Weight-based, low-dose pediatric whole-body PET/CT protocols. *J Nucl Med.* 2009;50(10):1570–7.
4. Uslu L, et al. Value of 18F-FDG PET and PET/CT for evaluation of pediatric malignancies. *J Nucl Med.* 2015;56(2):274–86.
5. Vali R, et al. SNMMI procedure standard/EANM practice guideline on pediatric (18)F-FDG PET/CT for oncology 1.0. *J Nucl Med.* 2021;62(1):99–110.
6. Bicakci N, Elli M. (18)Fluorine-fluorodeoxyglucose PET/CT imaging in childhood malignancies. *Mol Imaging Radionucl Ther.* 2021;30(1):18–27.
7. Daube-Witherspoon ME, Cherry SR. Scanner design considerations for long axial field-of-view PET systems. *PET Clin.* 2021;16(1):25–39.
8. Shammas A, Lim R, Charron M. Pediatric FDG PET/CT: physiologic uptake, normal variants, and benign conditions. *Radiographics.* 2009;29(5):1467–86.
9. Bestic JM, Peterson JJ, Bancroft LW. Pediatric FDG PET/CT: physiologic uptake, normal variants, and benign conditions [corrected]. *Radiographics.* 2009;29(5):1487–500.
10. Agrawal A, et al. PET/CT normal variants and pitfalls in pediatric disorders. *Semin Nucl Med.* 2021;51(6):572–83.
11. Bar-Sever Z, et al. Guidelines on nuclear medicine imaging in neuroblastoma. *Eur J Nucl Med Mol Imaging.* 2018;45(11):2009–24.
12. Rafael MS, et al. Theranostics in neuroblastoma. *PET Clin.* 2021;16(3):419–27.
13. Matthay KK, et al. Criteria for evaluation of disease extent by (123)I-metaiodobenzylguanidine scans in neuroblastoma: a report for the International Neuroblastoma Risk Group (INRG) task force. *Br J Cancer.* 2010;102(9):1319–26.
14. Sharp SE, et al. MIBG in neuroblastoma diagnostic imaging and therapy. *Radiographics.* 2016;36(1):258–78.
15. Bozkurt MF, et al. Guideline for PET/CT imaging of neuroendocrine neoplasms with (68)Ga-DOTA-conjugated somatostatin receptor targeting peptides and (18)F-DOPA. *Eur J Nucl Med Mol Imaging.* 2017;44(9):1588–601.
16. Chondrogiannis S, et al. Normal biodistribution pattern and physiologic variants of 18F-DOPA PET imaging. *Nucl Med Commun.* 2013;34(12):1141–9.
17. Calabria FF, et al. 18F-DOPA PET/CT physiological distribution and pitfalls: experience in 215 patients. *Clin Nucl Med.* 2016;41(10):753–60.
18. Hofman MS, Lau WF, Hicks RJ. Somatostatin receptor imaging with 68Ga DOTATATE PET/CT: clinical utility, normal patterns, pearls, and pitfalls in interpretation. *Radiographics.* 2015;35(2):500–16.
19. Sanli Y, et al. Neuroendocrine tumor diagnosis and management: (68)Ga-DOTATATE PET/CT. *AJR Am J Roentgenol.* 2018;211(2):267–77.
20. Stauss J, et al. Guidelines for paediatric bone scanning with 99mTc-labelled radiopharmaceuticals and 18F-fluoride. *Eur J Nucl Med Mol Imaging.* 2010;37(8):1621–8.
21. Segall G, et al. SNM practice guideline for sodium 18F-fluoride PET/CT bone scans 1.0. *J Nucl Med.* 2010;51(11):1813–20.
22. Eary JF, Conrad EU. Imaging in sarcoma. *J Nucl Med.* 2011;52(12):1903–13.
23. Beheshti M, et al. (18)F-NaF PET/CT: EANM procedure guidelines for bone imaging. *Eur J Nucl Med Mol Imaging.* 2015;42(11):1767–77.
24. Van den Wyngaert T, et al. The EANM practice guidelines for bone scintigraphy. *Eur J Nucl Med Mol Imaging.* 2016;43(9):1723–38.
25. Nadel HR. SPECT/CT in pediatric patient management. *Eur J Nucl Med Mol Imaging.* 2014;41(Suppl 1):S104–14.
26. Miller E, et al. Role of 18F-FDG PET/CT in staging and follow-up of lymphoma in pediatric and young adult patients. *J Comput Assist Tomogr.* 2006;30(4):689–94.
27. Howman-Giles R, London K, Uren RF. Solid tumors in childhood. In: Treves ST, editor. *Pediatric nuclear medicine and molecular imaging.* New York: Springer; 2014. p. 513–40.
28. Ferrari C, et al. Pediatric Hodgkin lymphoma: predictive value of interim 18F-FDG PET/CT in therapy response assessment. *Medicine (Baltimore).* 2017;96(5):e5973.
29. Kim K, Kim SJ. Diagnostic performance of F-18 FDG PET/CT in the detection of bone marrow involvement in paediatric Hodgkin lymphoma: a meta-analysis. *Leuk Res.* 2021;102:106525.
30. Barrington SF, Kluge R. FDG PET for therapy monitoring in Hodgkin and non-Hodgkin lymphomas. *Eur J Nucl Med Mol Imaging.* 2017;44(Suppl 1):97–110.
31. Hawkins DS, et al. [18F]Fluorodeoxyglucose positron emission tomography predicts outcome for Ewing sarcoma family of tumors. *J Clin Oncol.* 2005;23(34):8828–34.
32. Kubo T, et al. Prognostic significance of (18)F-FDG PET at diagnosis in patients with soft tissue sarcoma and bone sarcoma; systematic review and meta-analysis. *Eur J Cancer.* 2016;58:104–11.
33. Harrison DJ, Parisi MT, Shulkin BL. The role of (18)F-FDG-PET/CT in pediatric sarcoma. *Semin Nucl Med.* 2017;47(3):229–41.

34. London K, et al. 18F-FDG PET/CT in paediatric lymphoma: comparison with conventional imaging. *Eur J Nucl Med Mol Imaging*. 2011;38(2):274–84.
35. Cerci JJ, et al. Is true whole-body (18)F-FDG PET/CT required in pediatric lymphoma? An IAEA multicenter prospective study. *J Nucl Med*. 2019;60(8):1087–93.
36. Benz MR, Crompton JG, Harder D. PET/CT variants and pitfalls in bone and soft tissue sarcoma. *Semin Nucl Med*. 2021;51(6):584–92.
37. Swift CC, et al. Updates in diagnosis, management, and treatment of neuroblastoma. *Radiographics*. 2018;38(2):566–80.
38. Körber F, Schäfer JF. [Radiological imaging of neuroblastoma]. *Radiologe*. 2021;61(7):639–48.
39. Yanik GA, et al. Semiquantitative mIBG scoring as a prognostic indicator in patients with stage 4 neuroblastoma: a report from the Children's oncology group. *J Nucl Med*. 2013;54(4):541–8.
40. Yanik GA, et al. Validation of postinduction curie scores in high-risk neuroblastoma: A Children's Oncology Group and SIOPEX Group Report on SIOPEX/HR-NBL1. *J Nucl Med*. 2018;59(3):502–8.
41. Ladenstein R, et al. Validation of the mIBG skeletal SIOPEX scoring method in two independent high-risk neuroblastoma populations: the SIOPEX/HR-NBL1 and COG-A3973 trials. *Eur J Nucl Med Mol Imaging*. 2018;45(2):292–305.
42. Pai Panandiker AS, Coleman J, Shulkin B. Whole-body pediatric neuroblastoma imaging: 123I-mIBG and beyond. *Clin Nucl Med*. 2015;40(9):737–9.
43. Sharp SE, et al. Functional-metabolic imaging of neuroblastoma. *Q J Nucl Med Mol Imaging*. 2013;57(1):6–20.
44. Masselli G, et al. Clinical application of (18)F-DOPA PET/TC in pediatric patients. *Am J Nucl Med Mol Imaging*. 2021;11(2):64–76.
45. Pfluger T, Piccardo A. Neuroblastoma: MIBG imaging and new tracers. *Semin Nucl Med*. 2017;47(2):143–57.
46. Piccardo A, et al. Diagnosis, treatment response, and prognosis: the role of (18)F-DOPA PET/CT in children affected by neuroblastoma in comparison with (123)I-mIBG scan: the first prospective study. *J Nucl Med*. 2020;61(3):367–74.
47. Lopci E, et al. 18F-DOPA PET/CT in neuroblastoma: comparison of conventional imaging with CT/MR. *Clin Nucl Med*. 2012;37(4):e73–8.
48. Kong G, et al. Initial experience with Gallium-68 DOTA-octreotate PET/CT and peptide receptor radionuclide therapy for pediatric patients with refractory metastatic neuroblastoma. *J Pediatr Hematol Oncol*. 2016;38(2):87–96.
49. Maaz AUR, O'Doherty J, Djekidel M. (68) Ga-DOTATATE PET/CT for neuroblastoma staging: utility for clinical use. *J Nucl Med Technol*. 2021;49(3):265–8.
50. Imperiale A, et al. Variants and pitfalls of PET/CT in neuroendocrine tumors. *Semin Nucl Med*. 2021;51(5):519–28.
51. Chondrogiannis S, Marzola MC, Rubello D. ¹⁸F-DOPA PET/computed tomography imaging. *PET Clin*. 2014;9(3):307–21.
52. Piccardo A, et al. Head-to-head comparison between (18) F-DOPA PET/CT and (68) Ga-DOTA peptides PET/CT in detecting intestinal neuroendocrine tumours: a systematic review and meta-analysis. *Clin Endocrinol (Oxf)*. 2021;95(4):595–605.
53. Adzick NS, et al. Surgical treatment of congenital hyperinsulinism: results from 500 pancreatectomies in neonates and children. *J Pediatr Surg*. 2019;54(1):27–32.
54. Bartel TB, et al. SNMMI procedure standard for bone scintigraphy 4.0. *J Nucl Med Technol*. 2018;46(4):398–404.
55. Usmani S, et al. Technical feasibility, radiation dosimetry and clinical use of (18)F-sodium fluoride (NaF) in evaluation of metastatic bone disease in pediatric population. *Ann Nucl Med*. 2018;32(9):594–601.
56. Vaz S, et al. Molecular imaging of bone metastases using bone targeted tracers. *Q J Nucl Med Mol Imaging*. 2019;63(2):112–28.

The opinions expressed in this chapter are those of the author(s) and do not necessarily reflect the views of the IAEA: International Atomic Energy Agency, its Board of Directors, or the countries they represent.

Open Access This chapter is licensed under the terms of the Creative Commons Attribution 3.0 IGO license (<http://creativecommons.org/licenses/by/3.0/igo/>), which permits use, sharing, adaptation, distribution and reproduction in any medium or format, as long as you give appropriate credit to the IAEA: International Atomic Energy Agency, provide a link to the Creative Commons license and indicate if changes were made.

Any dispute related to the use of the works of the IAEA: International Atomic Energy Agency that cannot be settled amicably shall be submitted to arbitration pursuant to the UNCITRAL rules. The use of the IAEA: International Atomic Energy Agency's name for any purpose other than for attribution, and the use of the IAEA: International Atomic Energy Agency's logo, shall be subject to a separate written license agreement between the IAEA: International Atomic Energy Agency and the user and is not authorized as part of this CC-IGO license. Note that the link provided above includes additional terms and conditions of the license.

The images or other third party material in this chapter are included in the chapter's Creative Commons license, unless indicated otherwise in a credit line to the material. If material is not included in the chapter's Creative Commons license and your intended use is not permitted by statutory regulation or exceeds the permitted use, you will need to obtain permission directly from the copyright holder.

